Pergamon

Trace element incorporation into quartz: A combined study by ICP-MS, electron spin resonance, cathodoluminescence, capillary ion analysis, and gas chromatography

JENS GÖTZE,[1,*] MICHAEL PLÖTZE,[2] TORSTEN GRAUPNER,[3] DIETER KLAUS HALLBAUER,[4] and COLIN J. BRAY[5]

[1]TU Bergakademie Freiberg, Department of Mineralogy, Brennhausgasse 14, D-09596 Freiberg, Germany
[2]ETH Zürich, IGT ClayLab, CH-8093 Zürich, Switzerland
[3]Universität Würzburg, Department of Mineralogy, Am Hubland, D-97074 Würzburg, Germany
[4]University of Stellenbosch, Department of Geology, Private Bag X1, Matieland 7602, Republic of South Africa
[5]University of Toronto, Department of Geology, 22 Russell Street, Toronto, Ontario, M5S 3B1, Canada

Abstract—Pegmatite quartz from different occurrences in Norway and Namibia was investigated by a combination of ICP-MS, Electron Spin Resonance (ESR), Capillary Ion Analysis (CIA) and Gas Chromatography (GC) to quantify trace elements in very low concentrations and to determine their position in the quartz structure.

The studied quartz samples show similar geochemical characteristics with low contents of most trace elements. Remarkable are the elevated concentrations of Al (36–636 ppm), Ti (1.6–25.2 ppm), Ge (1.0–7.1 ppm), Na (5.2 to >50 ppm), K (1.6 to >100 ppm) and Li (2.1–165.6 ppm). These elements are preferentially incorporated into the quartz lattice on substitutional (Al, Ti, Ge) and interstitial (Li, Na, K) positions. Li^+ was found to be the main charge compensating ion for Al, Ge and Ti, whereas some ppm of Na and K may also be hosted by fluid inclusions. Ti may be incorporated as substitutional ion for Si or bound on mineral microinclusions (rutile). The results of the ESR measurements show that there may be a redistribution of alkali ions during irradiation. The diamagnetic $[AlO_4/M^+]^0$ center transforms into the paramagnetic $[AlO_4]^0$ center, whilst the compensating ions diffuse away and may be captured by the diamagnetic precursor centers of $[GeO_4]^0$ and $[TiO_4]^0$ to form paramagnetic centers ($[TiO_4/Li^+]^0$, $[GeO_4/Li^+]^0$).

In general, fluid inclusions in pegmatite quartz can be classified as H_2O-CO_2-NaCl type inclusions with water as the predominant volatile. Among the main elements hosted by fluid inclusions in quartz are Na, K, NH_4, Ca, Mg and the anionic complexes Cl^-, NO_3^-, HCO_3^- and SO_4^{2-}. Gas analysis of trapped fluids shows volatile components in the following order of abundance: $H_2O > CO_2 > N_2(+) \geq CH_4 > COS > C_2$ and C_3 hydrocarbons. Additionally, traces of Co, Ni, Zn, Pb, and Cu were detected by CIA in fluid inclusions of some samples. There are indications that the REE and Rb are also bound in fluid inclusions, however, the concentrations of these elements are too low to be measured by CIA. Assuming that the REE preferentially occur in fluid inclusions, the typical chondrite normalized REE distribution patterns with tetrad effects and a distinct negative Eu anomaly would reflect the composition of the mineralizing fluid.

For a number of elements, especially those with extremely low concentrations, the "type" of incorporation in quartz could not directly be determined. We conclude that these ions either are too large to substitute for the small Si^{4+} ion or they are not soluble in the mineralizing fluids to be hosted by fluid inclusions. Some of these elements, which are concentrated in the specific mineralization of certain pegmatites, are not present in elevated concentrations in the paragenetic pegmatite quartz itself. This was observed, for instance, for Be, Cs and Rb in the Li (Be-Cs-Rb) pegmatites of Rubicon or for Nb and Ta for Nb-Ta bearing pegmatites from Norway. It may be concluded that the concentrations of these trace elements in quartz do not reflect the mineralization and that these elements thus, cannot be used as petrogenetic indicator. *Copyright © 2004 Elsevier Ltd*

1. INTRODUCTION

Trace elements in minerals are considered important petrogenetic indicators for interpreting the conditions of mineral formation, to reveal the provenance of minerals, or to reconstruct the genesis of ore deposits and the origin of metal-bearing fluids. Because of the widespread occurrence of quartz in igneous, metamorphic and sedimentary rocks, several attempts have been made to use trace elements for genetic interpretations (e.g., Bambauer, 1961; Dennen, 1964, 1966, 1967; Walenczak, 1969; Lyakhovich, 1972; Suttner and Leininger, 1972; Hallbauer, 1992; Heynke et al., 1992; Götze and

Lewis, 1994; Götze and Plötze, 1997; Monecke et al., 1999, 2002a; Götze and Zimmerle, 2000; Larsen et al., 2000; Poutivcev et al., 2001; Müller et al., 2003).

For detailed interpretation, different mechanisms of trace element uptake into the quartz lattice have to be discussed. Trace elements in quartz may generally be incorporated into the crystal structure or bound to microinclusions (fluid or mineral inclusions). Due to its structure and the small size of the Si^{4+} ion (0.42 Å), quartz is considered to incorporate only small amounts of "foreign" elements into its crystal lattice. The substitutional incorporation of Al, Ge, Ti, Ga, Fe, H and P into the Si position is well established (e.g., Weil, 1984, 1993). If necessary, the charge deficit is compensated by cations, which are distributed in structural channels parallel to the c-axis. Cations which were detected on interstitial lattice positions are

---

* Author to whom correspondence should be addressed (goetze@mineral.tu-freiberg.de).

Table 1. Pegmatite samples from different occurrences selected for the present study.

Sample		Location	Mineralization	Microscopic characteristics
Qz1a	quartz	Frikstad	quartz, feldspar, mica,	bottle-green cathodoluminescence (CL)
Qz1b	smoky quartz	Evje-Iveland, Norway	Nb/Ta, REE, gadolinite, garnet	bottle-green CL, subcrystals
Qz2a	quartz	Skavdalen	quartz, feldspar (graphic granite),	homogeneous bluish-green CL, fluid trails
Qz2b	smoky quartz	Evje-Iveland, Norway	monazite, garnet	homogeneous bluish-green CL, fluid trails
Qz3a	quartz	Brattekleiv	quartz, feldspar (amazonite),	bluish-green CL with dark fluid trails
Qz3b	smoky quartz	Evje-Iveland, Norway	beryl, Nb/Ta, garnet	bluish-green CL with dark fluid trails
Qz4a	quartz	Våanne	quartz, feldspar, mica,	homogeneous bottle-green CL, subcrystals
Qz4b	smoky quartz	Evje-Iveland, Norway	monazite, garnet	homogeneous bottle-green CL, fluid trails
Qz5a	quartz	Steli near Dalane	quartz, feldspar, mica, monazite,	homogeneous bottle-green CL
Qz5b	smoky quartz	Evje-Iveland, Norway	garnet (pseudomorphs after mica)	homogeneous bluish CL, chlorite
Qz6a	quartz	Li	feldspar (perthitic),	homogeneous bluish green CL, rutile
Qz6b	smoky quartz	Evje-Iveland, Norway	quartz	bluish-green CL, fluid trails, chlorite
Qz7a	quartz	Drag	quartz, feldspar (amazonite), mica,	greenish-blue CL, subcrystals, biotite
Qz7b	smoky quartz	Norway	fluorite, garnet, Nb/Ta, REE	homogeneous greenish-blue CL
Qz9a	quartz	Hittero Hitra, Norway	quartz, feldspar, mica, Nb/Ta, Th, REE	bluish-green CL, fluid trails
Qz15a	quartz	Rubicon Mine	quartz, feldspar, (Li-) muscovite,	bluish CL, brighter luminescing fluid trails
Qz15b	smoky quartz	Namibia	petalite, lepidolite, garnet,	bluish CL, brighter luminescing fluid trails
Qz15c	rose quartz		amblygonite, columbite	bluish CL, brighter luminescing fluid trails

commonly the alkali ions Li^+, Na^+, K^+ and H^+, but also include the ions of Cu, Ag, Al, Fe, Ti, Co, Cr, Ni (Weil, 1984, 1993).

For most elements in quartz, however, their capture by microinclusions is most important (Blankenburg et al., 1994). Jung (1992) suggested that only Al, B, Ge, Fe, H, K, Li, Na, P and Ti are structurally incorporated, whereas Ca, Cr, Cu, Mg, Mn, Pb, Rb and U occur in solid and liquid inclusions. Rossman et al. (1987) proved that Sr, Rb, Sm, Nd are mostly not structurally incorporated into quartz and discussed the role of fluid inclusions in hosting these elements. Gerler (1990) showed a strong correlation of the elements Cl, Br, Na, Ca, Sr, and Mn with the water content of fluid inclusions and concluded that up to 100% of Cl, Br and I may be concentrated there. Other elements which were detected in fluid inclusions of quartz are Ag, Au, K, Li, F, Mg, Ba, Cs, B, Hg, Fe, Co, Cu, Pb, Sb, Zn and U (e.g., Czamanske et al., 1963; Suščevskaya et al., 1970; Pickney and Haffty, 1970; Malinko et al., 1976; Baranova et al., 1980; Naumov et al., 1984; Gerler and Schnier, 1989; Klemm, 1994). On the other hand, Gerler (1990) found that the elements K, Cs, Rb, Fe, Cr, Co, Al, Ba, Sc, W, U and the REE can also be related to microscopic mineral inclusions in quartz. This illustrates that the mechanisms of incorporation may be variable, even for a specific element in a single crystal.

In general, it is difficult to quantify the amounts of differently incorporated trace elements, and it is impossible if only one analytical method is used. Therefore, an attempt was made in the present study to quantify the distribution of trace elements in quartz by a combination of ICP-MS, Capillary Ion Analysis (CIA) and Electron Spin Resonance (ESR). ICP-MS is a powerful method for the detection of the very low concentrations of many trace elements in bulk quartz specimens. CIA can be applied to the analysis of a wide variety of cations and anionic complexes in fluids in the lower ppb range. Thus, this method enables to reveal separately the trace element concentrations bound in fluid inclusions of minerals. The application of ESR enables the detection of such trace elements, which are incorporated into the quartz lattice forming a paramagnetic center. The combination of these methods provides more in-

formation about the mechanism of trace element uptake in quartz than application of any single method could.

2. MATERIALS AND METHODS

2.1. Sample Material

The material investigated includes 18 samples of pegmatite quartz from Norway and Namibia (Table 1). Quartz from pegmatites was selected to obtain enough sample material of pure quartz for the different analytical techniques.

Both quartz and smoky quartz were sampled from the pegmatite bodies of Frikstad, Skavdalen, Brattekleiv, Vanne, Steli near Dalane and Li, which all belong to the pegmatite complex of Evje-Iveland in Southern Norway (Bjørlykke, 1934). The igneous activity in this region took place ~1250 Ma ago and was associated with crustal extension and formation of basic and felsic igneous rocks (Pedersen, 1981). Large-scale emplacement of posttectonic undeformed plutons took place at ca. 1000 Ma with massive granite, monzonite and diorite emplacement. Geochronological studies of the Evje-Iveland pegmatites provided an age of 852 ± 12 Ma based on Rb-Sr dating of K-feldspar (Stockmarr, 1994). The bodies of granitic pegmatites in Evje-Iveland comprise classical zoned "chamber" pegmatites that mostly crystallized as subvertical or subhorizontal dikes or sills, respectively (Larsen, 2002). They rarely exceed 20 m in thickness and have lateral extent of less than 100 m. It was suggested that the coarse-grained granitic pegmatites of Evje-Iveland formed from progressively more differentiated melts that were emplaced in a southward-propagating system of vertical and horizontal faults and fractures within mafic host rocks (amphibolite, norite, mafic gneiss) (Larsen, 2002). The samples represent different localities of quartz in one pegmatite province, consisting above all of quartz-feldspar(-mica) pegmatites that have partly REE-Nb-Ta-Be (e.g., gadolinite, beryl, monazite, allanite, tantalite, magnetite, spessartine) mineralization.

Additional samples were taken from the quartz-feldspar pegmatite of Drag, Norway and the pegmatite of Hitterø, Norway, which are characterized by Nb-Ta(-Th) mineralization (Oftedahl, 1980). The locality of Drag is situated in the Tysfjord area in the northern part of Norway. The pegmatite body was formed ~1800 million years ago, when granites intruded 2500 Ma old gneisses. The zoned pegmatite of Drag developed from a mixed pegmatite of feldspars, quartz and mica to smoky quartz and coarse grained, pure quartz; the latter is partly associated with fluorite (Table 1). The granitic pegmatite of Hitterø on Hidra Island belongs to the ~930 Ma old Rogaland anorthosite province. Recent results have indicated that the melts of this large Proterozoic igneous complex derived from lower continental crust (Schiellerup

et al., 2000). The mineralization of the pegmatite includes, besides quartz, feldspars and mica, also Nb/Ta-, Th- and REE minerals.

Furthermore, material (quartz, smoky quartz and rose quartz) from the Rubicon mine, located 30 km SE of Karibib, Namibia, was studied. This pegmatite represents a group of Li-Cs-Be-Rb pegmatites that belong to the Okongava granite, which intruded at 515 Ma ago (ca. 720 Ma) diorites of the Damara complex. Field observations and results of mineralogical investigations indicated that the genesis of these pegmatites can be related to dome structures and diorites of the Goas Suite (Keller, 1999). The gently dipping pegmatites developed from a probably prefractionated fluid-rich granite and occur on the margin of diorites, which could have acted as a barrier for the fluids. Although the pegmatites, in general, reached a high degree of alkali fractionation (e.g., petalite, pollucite mineralization), the pegmatite of Rubicon itself does not show intensive fractionation trends, which was interpreted to reflect continuous metasomatic processes at high temperatures (Keller, 1999). In Table 1 the main mineralizations of the sampled pegmatites are summarized.

The preparation of pure quartz samples was preceded by mineralogical investigations on thin sections to reveal impurities in the quartz material to be analyzed and to study possible internal structures. Features such as strain domains, subgrain boundaries, and others, may indicate areas of enhanced accommodation of fluid and mineral inclusions. Polished thin sections were investigated by conventional polarized microscopy, cathodoluminescence (CL) microscopy (hot-cathode CL microscope HC1-LM), and scanning electron microscopy (SEM) using a JEOL 6400 with a Noran EDX detector. The CL technique proved to be particularly useful to identify minute inclusions of apatite, fluorite, calcite and feldspar, because of their bright CL and characteristic luminescence colors. The search for sheet silicates and Fe-Ti oxides was done by SEM. The studies confirmed that the specimens mainly consist of large zones of pure quartz that could be sampled by hand-picking. Solid inclusions other than rutile are rare in the samples. Rutile may occur as minute submicron-thick needles, which are dispersed throughout the quartz. Additionally, tiny inclusions of chlorite (in sample Qz5b/6b), pyrophyllite (Qz6b), biotite and fluorite (Qz7a) were detected; these were always arranged outlining secondary microcracks. The quartz samples were crushed in an agate mortar, and pure quartz grains without visible impurities were hand-picked under a binocular microscope. The separated fractions were repeatedly washed with 2 mol/L nitric acid and ultrapure water, and then air dried.

2.2. Analytical Procedure

The samples (400–500 mg) for ICP-MS analysis were milled to a grain size of ~30 μm using a precleaned agate mortar. The powdered sample was digested in a glassy carbon vessel with 5 mL concentrated HF and 3 mL concentrated HNO_3 at 50°C (35 min). Rhenium solution (1 mL of 100 μg/L concentration) was added as an internal standard for the ICP-MS measurements. The analysis was performed using a Perkin Elmer Sciex Elan 5000 quadrupole instrument with a cross-flow nebulizer and a rhyton spray chamber. The precision and accuracy of the ICP-MS measurements were evaluated by analysis of the glass sand reference material UNS-SpS. The relative standard deviations for most analytes were below 10%. The ICP-MS results showed procedural limits of detection ranging from 0.22 to 3.1 μg L^{-1} for Na, Mg, Al, K, Ca and Ba. Elements such as Li, Mn and Sr had procedural limits of detection of 0.02 to 0.04 μg L^{-1}, whereas these limits range from 1 to 7 ng L^{-1} for the other elements investigated (Monecke et al., 2000).

Fluid inclusions were examined using a Linkam THMS 600 heating-freezing stage. Two synthetic fluid inclusion standards (SYN FLINC; pure H_2O, mixed H_2O-CO_2) were used to calibrate the equipment. The precision of the system was ±2 °C for homogenization temperatures (Th), and ±0.2 °C in the temperature range between −60 and +10 °C.

Analysis of trace elements in fluid inclusions was carried out by Capillary Ion Analysis (CIA). The separation of different cations and anionic complexes for analysis is based on the different electrophoretic mobilities of the hydrated or complexed species, or their charge/mass ratio in an electrolyte moving through a fused silica capillary in an electric field. The detection is accomplished at the end of the capillary by indirect UV detection (Hallbauer, 1997).

CIA analyses were carried out using a WATERS Quanta 4000 instrument coupled with a digital to analog converter for computer-

aided data processing. Sampling of the UV detector output was set at 50 Hz intervals or 0.02 s intervals. All quantitative calculations are based on peak area integrations. Detection limits in the ppb region can be achieved using the electromigration mode (Hallbauer, 1997).

A specific procedure for the extraction of fluid inclusions from samples by crushing and leaching had to be designed because of the behavior of fluid inclusions and the adsorption and consequent loss of ionic species onto fresh fracture surfaces (Bottrell et al., 1988; Yardley et al., 1993). In the present study a crush and leach method, with leaching in 2.5 mL of MQ water with Tetrabutylammonium Hydroxide (TBA) with subsequent pass through a 0.47 μm membrane filter, was used (Hallbauer, 1997). Deionized water supplied by a Milli-Q system (Millipore, Bedford, MA, USA) was used for these experiments. The water blank is routinely checked for contamination and varied between 0.5 and 1 ppb K, Na and Ca. A 10 mM pyridine electrolyte was used for cation separations (60 cm capillary, 25 kV separation voltage) with 25 mM glycolic acid as a general complexing agent, resulting in a pH value of ~4.5. To separate the comigrating cations of K and NH_4, a further addition of 1 mM "crown" ether (Jandik and Bonn, 1993) for complexation of K cation was found to be sufficient.

For the determination of anionic species a separate capillary was used and specially conditioned for use with an osmotic flow modifier (OFM). A convenient co-ion and chromofore is chromate (Jandik and Bonn, 1993), which was prepared from sodium chromate tetra hydrate as a 5 mM solution with a pH of ~8.0, adjusted by sulfuric acid. Best separations were achieved at ~20 kV.

CL spectra were obtained on carbon-coated polished thin sections using a CL microscope with an EG&G digital triple-grating spectrograph and a liquid nitrogen cooled CCD detector in the range 380–1000 nm (VIS-IR). To prevent distortion of the spectra by prolonged exposure to the electron beam, all spectra were taken on nonirradiated sample spots. Time-resolved (20 × 5 s) CL spectra were measured on selected samples to study the CL behavior of the minerals during electron irradiation. In addition, spectral CL investigations were carried out using a JEOL JSM 6400 SEM equipped with an Oxford MonoCL system over the range 200–800 nm (UV-VIS). For CL investigations, the accelerating voltage was set at 20 kV and the beam current in the range 0.6–1.6 nA.

Bulk volatile compositions of fluids trapped in inclusions were analyzed by gas chromatographic (GC) analysis (Bray et al., 1991; Channer et al., 1999). A sample mass of ~1.2 g was used. To quantify trace element ratios measured by CIA and to calculate the salinity of the extracted fluids, the water content in the samples was calculated using the results of the gas chromatographic analysis.

The paramagnetic centers of irradiated quartz powder samples were investigated by Electron Spin Resonance (ESR) at frequencies of the X-band (9.5 GHz) at 70 and 295 K. The quartz grains were carefully crushed to a size < 200 μm, in an agate mortar under ethanol and dried at 25 °C. The samples were γ-irradiated (^{60}Co, 295 K, 1.4 × 10^4 Gy ± 10%) to transform the trace element defects from the nonparamagnetic precursor state into paramagnetic centers. Center saturation was achieved at 1 × 10^4 Gy for [GeO$_4^-$/M$^+$]^0 and [TiO$_4^-$/Li$^+$]^0 and at 1 × 10^6 Gy for [AlO$_4$]^0 (Plötze, 1995; Plötze and Wolf, 1996). Before irradiation, the samples were heated at 400 °C for 5 h to anneal the paramagnetic centers formed by natural irradiation. Spectra were recorded with a Bruker cw-spectrometer (ESP300E and ElexSys E500, respectively). Sample temperature was controlled with a low temperature unit based on a helium gas flow device (Oxford ESR 900A). The influence of technical parameters such as modulation amplitude, microwave power, temperature, scan time, etc., on the spectra was checked for the optimal settings for recording the spectra. These settings (sample mass 150 mg, modulation field H_M = 1 G, temperature T = 295 K, microwave power p = 10 mW for Fe^{3+} and [GeO$_4^-$/M$^+$]^0 centers and H_M = 1 G, p = 7 mW, T = 70 K for [AlO$_4$]^0 and [TiO$_4^-$/Li$^+$]^0 centers) were kept constant throughout all the measurements to allow comparison between the signal intensities of different spectra. The concentrations of the paramagnetic centers were determined as peak to peak or peak to base intensity at the analytical lines (Moiseev, 1985). The specific peak positions of the paramagnetic centers were drawn from simulated spectra and from data from the literature. The program of Nettar and Villafranca (1985) was used for the powder spectra simulations. The variation of intensity detected by repeated measurements of selected analytical lines is up to 10%. The

Table 2. Trace-element composition of investigated quartz samples from pegmatites (results in ppm).[a]

	1a	1b	2a	2b	3a	3b	4a	4b	5a	5b	6a	6b	7a	7b	9a	15a	15b
Ag	0.019	0.003	0.003	0.002	0.002	0.008	0.017	0.011	0.002	0.002	0.001	0.001	0.001	0.011	0.001	0.002	0.001
Al	518	129	112	262	106	65	201	78	106	143	134	178	41	36	64	636	324
B	13.7	0.52	0.41	0.35	0.54	0.51	1.03	0.44	0.26	0.36	0.39	0.82	0.68	0.61	0.27	1.72	0.59
Ba	1.49	0.46	0.39	0.39	0.49	0.39	0.54	0.65	0.31	0.31	0.46	0.37	0.27	0.46	0.37	0.47	0.13
Be	0.22	0.14	0.18	0.38	0.16	0.15	0.39	0.26	0.11	0.18	0.03	0.34	0.13	0.06	0.12	0.37	0.06
Ca	31.9	10.4	11.2	9.54	8.34	7.38	30.8	17.6	10.5	6.78	8.07	13.5	6.04	7.01	20.4	8.34	8.59
Cd	0.007	0.001	0.002	0.002	0.002	nd	0.015	0.011	0.003	0.004	0.004	0.007	0.003	0.008	0.002	0.004	0.002
Co	0.052	0.026	0.017	0.027	0.022	0.022	0.027	0.028	0.008	0.007	0.012	0.007	0.006	0.011	0.008	0.011	0.027
Cr	0.86	0.16	0.16	1.09	0.51	0.18	0.39	0.27	0.09	0.08	0.12	0.11	0.11	0.18	0.09	0.16	0.09
Cs	2.03	0.28	0.043	0.019	0.21	0.17	1.84	0.15	0.003	0.021	0.009	1.12	0.004	0.006	0.034	0.045	0.048
Cu	4.29	1.35	0.72	0.69	0.62	11.9	4.52	3.98	0.76	0.91	1.12	0.59	0.45	1.53	0.32	1.09	2.99
Fe	nd	1.26	1.45	5.68	2.09	1.15	nd	3.75	2.17	5.11	2.26	2.95	5.42	13.6	5.73	6.46	3.41
Ga	0.062	0.019	0.034	0.066	0.026	0.039	0.27	0.046	0.038	0.026	0.024	0.059	0.022	0.024	0.018	0.053	0.017
Ge	7.12	5.67	1.42	2.03	3.24	2.57	2.05	3.44	1.49	1.66	0.97	2.79	1.59	1.24	1.89	5.58	5.15
Hf	0.006	0.005	nd	nd	nd	nd	0.029	nd	nd	nd	nd	nd	nd	nd	nd	nd	0.003
K	24.3	4.91	9.12	>100	11.2	6.63	>100	9.04	7.51	>100	5.35	29.8	4.53	5.02	6.81	2.37	1.64
Li	33.9	26.1	11.5	8.41	4.92	8.52	3.33	6.06	17.9	6.81	6.54	24.1	6.47	2.96	2.09	165.6	56.4
Mg	8.77	1.65	1.77	2.27	1.29	1.08	15.7	8.58	1.99	1.79	1.88	1.55	1.04	1.57	1.47	1.27	0.74
Mn	1.15	0.34	0.37	0.66	0.31	0.25	3.24	0.44	0.27	0.25	0.23	1.41	0.15	1.03	0.64	0.37	0.14
Na	30.3	9.78	12.3	13.4	19.1	11.2	>50	13.1	10.3	14.9	8.61	>50	4.14	12.1	>50	5.89	5.16
Nb	0.12	0.005	0.009	0.012	0.005	0.004	0.23	nd	0.015	0.031	0.003	0.012	0.009	0.006	nd	nd	nd
Ni	6.35	2.96	1.18	1.94	2.13	1.66	2.69	3.75	1.28	1.01	1.78	0.94	0.82	1.45	1.37	1.64	5.56
Pb	0.78	0.15	0.31	0.31	0.16	0.36	0.61	0.52	0.11	0.13	0.14	0.34	0.44	0.19	0.11	0.17	0.08
Rb	0.91	0.12	0.19	0.26	0.29	0.04	7.36	0.22	0.03	0.25	0.03	1.27	0.05	0.061	0.13	0.029	0.009
Sb	0.025	0.038	0.009	0.008	0.093	0.114	0.083	0.019	0.003	0.038	0.003	0.084	0.026	0.012	0.005	0.098	0.037
Sc	0.006	nd	nd	nd	nd	nd	nd	nd	0.003	0.002	nd	0.003	0.036	nd	nd	nd	nd
Sn	0.12	0.19	0.034	0.043	0.031	1.13	0.11	0.039	0.021	0.038	0.027	0.029	0.031	0.054	0.018	0.016	0.017
Sr	0.29	0.13	0.077	0.058	0.12	0.083	0.11	0.11	0.044	0.059	0.081	0.14	0.033	0.091	0.55	0.045	0.037
Ta	0.14	0.005	nd	nd	nd	nd	0.25	nd	0.003	0.002	nd	0.006	0.011	nd	nd	nd	nd
Th	0.026	0.003	0.003	0.004	0.004	0.003	0.036	0.003	0.004	0.114	0.011	0.008	0.004	0.011	0.002	0.001	0.002
Ti	10.3	3.62	14.5	22.1	5.28	8.66	14.5	13.1	5.59	4.55	24.4	25.2	6.35	2.05	8.68	1.59	0.34
U	0.018	0.011	0.008	0.004	0.006	0.003	0.044	0.001	0.008	0.014	0.003	0.008	0.004	0.012	0.006	0.0008	0.0023
V	0.075	0.009	0.013	nd	0.016	0.009	0.049	0.026	0.009	0.009	0.009	0.009	nd	nd	nd	nd	nd
Y	0.043	0.012	0.009	0.008	0.029	0.016	0.079	0.011	0.008	0.039	0.006	0.025	0.007	0.019	0.16	0.0045	0.0026
Zn	2.64	0.76	0.54	0.64	0.55	0.51	4.06	2.01	0.76	3.84	0.81	0.71	0.46	0.79	0.55	1.17	1.63
Zr	0.18	0.05	0.02	0.02	0.03	0.03	0.13	0.039	0.018	0.012	0.018	0.015	0.016	0.024	0.005	0.012	0.028

[a] nd = below detection limit.

concentration of Al centers was quantified using a reference sample with known $[AlO_4]^0$ concentration (Moiseev, 1985). All other centers were calculated in relative amounts.

3. RESULTS

3.1. Bulk Trace Element Composition

In general, quartz of pegmatitic origin is characterized by uniform geochemical characteristics with low contents of most trace elements (Tables 2 and 3). Remarkable are the elevated concentrations of Al (41–636 ppm), Ti (0.3–25.2 ppm), Ge (1.0–7.1 ppm), Na (5.2 to >50 ppm), K (1.6 to >100 ppm) and Li (2.1–165.6 ppm). A characteristic feature of quartz from pegmatites is a high Ge/Fe ratio (4.5–0.1) compared to quartz samples of other origin. According to Schrön et al. (1982), quartz of early crystallization stages is characterized by low Ge/Fe ratios (high iron content), whereas this ratio is high in quartz of late generations. Therefore, pegmatitic mineralization has in general high Ge and low Fe contents and may show

Table 3. Concentrations of REE (in ppb) and chondrite-normalized interelemental ratios of the investigated quartz samples.[a]

	1a	1b	2a	2b	3a	3b	4a	4b	5a	5b	6a	6b	7a	7b	9a	15a	15b	15c
La	62.2	16.1	15.9	12.5	17.1	14.9	32.4	14.4	9.7	55.4	15.2	19.1	6.2	10.3	10.3	7.8	4.3	5.1
Ce	134	31.1	30.9	27.4	43.2	36.3	96.8	33.2	24.1	162	31.4	40.8	15.2	14.3	33.2	16.2	7.2	9.9
Pr	11.8	2.1	2.4	2.1	3.8	2.8	13.1	2.8	1.9	22.4	3.5	3.9	1.3	2.1	4.1	1.3	0.7	0.9
Nd	42.6	7.1	9.1	6.2	13.9	9.8	53.1	8.6	6.2	93.9	13.2	13.0	4.0	6.8	16.8	3.7	2.0	2.9
Sm	8.8	1.5	1.4	1.2	3.8	2.5	23.4	2.1	0.8	32.8	2.8	3.2	1.2	1.4	8.0	0.8	0.5	0.7
Eu	1.6	0.2	0.2	0.2	0.3	0.2	0.3	0.1	0.06	0.1	0.1	0.1	0.1	0.2	0.9	0.1	0.06	0.1
Gd	9.5	1.6	1.2	1.2	3.3	1.9	19.1	1.7	1.0	18.1	1.7	3.3	1.0	1.9	11.6	0.5	0.3	0.5
Tb	1.7	0.3	0.3	0.2	0.7	0.4	3.3	0.3	0.2	0.2	0.3	0.4	0.2	0.4	2.8	0.1	0.06	0.07
Dy	9.8	1.7	1.3	1.2	3.9	1.9	15.8	1.5	1.4	11.2	1.5	3.2	1.6	2.7	19.7	0.6	0.3	0.3
Ho	1.9	0.3	0.3	0.3	0.7	0.4	2.1	0.3	0.3	1.4	0.2	0.7	0.4	0.7	4.2	0.1	0.08	0.07
Er	5.4	1.1	0.9	0.9	2.3	1.2	5.8	1.0	0.8	3.9	0.6	2.4	1.5	2.3	14.6	0.5	0.3	0.25
Tm	0.9	0.2	0.2	0.2	0.5	0.3	0.9	0.2	0.2	0.6	0.1	0.4	0.3	0.4	3.0	0.1	0.03	0.05
Yb	5.4	0.9	1.2	1.1	4.1	2.2	8.0	0.8	1.2	5.2	0.6	3.6	3.2	2.8	27.9	0.4	0.2	0.3
Lu	0.9	0.2	0.2	0.2	0.6	0.4	1.2	0.1	0.2	0.7	0.2	0.6	0.6	0.5	4.2	0.1	0.03	0.02
Eu/Eu*	0.57	0.42	0.50	0.54	0.27	0.30	0.05	0.17	0.33	0.03	0.15	0.10	0.29	0.40	0.31	0.51	0.84	0.5
La_n/Yb_n	6.9	10.7	8.0	6.6	2.5	4.1	2.4	9.4	5.5	6.4	15.1	3.2	1.2	2.4	0.3	11.8	13.0	10.2
La_n/Sm_n	4.4	6.7	7.1	6.2	2.8	3.8	0.8	4.2	7.6	1.1	3.4	3.7	3.5	4.9	0.9	6.1	5.4	4.6
Gd_n/Yb_n	1.2	1.2	0.7	0.7	0.6	0.6	1.6	1.3	0.6	2.4	1.9	0.7	0.4	0.5	0.3	0.8	1.0	1.1

[a] The normalization is based on data given by Mason (1979); the Eu anomaly is defined as $Eu/Eu^* = Eu_n/(Sm_n \cdot Gd_n)^{0.5}$.
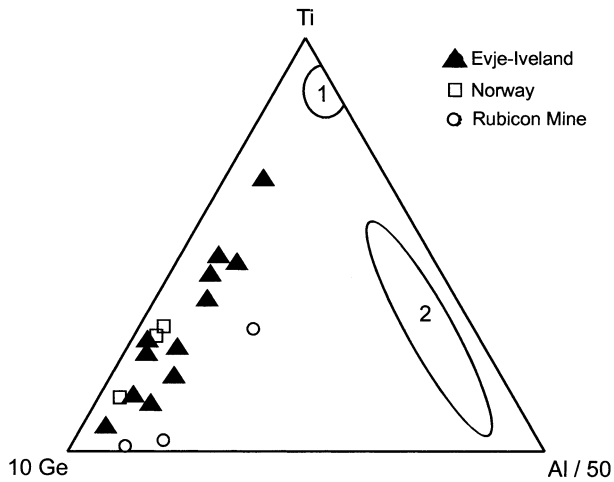
Fig. 1. 10Ge-Al/50-Ti diagram after Schrön et al. (1982). The pegmatite quartz samples of this study plot within a field far from the trace element composition of quartz from rhyolites (1) and granites (2).

variations of the Ge/Fe ratio which relate to the crystallization sequence.

The Ge speciation is also illustrated in the 10Ge-Al/50-Ti diagram (Fig. 1) The samples plot within a field far from the trace element composition of granite and rhyolite quartz, respectively. The high Ge content is a characteristic feature of quartz from pegmatite bodies and was also observed in quartz from pegmatites of other regions (Schrön et al., 1988a).

Although the quartz samples from the different occurrences vary in absolute concentrations of several trace elements, they show some general trends in trace element ratios (Fig. 2). The quartz samples from the Li (Be-Cs-Rb) pegmatite of Rubicon have high contents of Al, Li and Ge, but, in contrast, contain very low concentrations of K, Na, Rb, Sr, Cs, U and Th. The concentrations of Nb, Sc and Ta are below the detection limit of the trace element analysis. This is interesting in so far as the Be-Cs-Rb mineralization of the pegmatite does not seem to influence the trace element composition of the quartz. A similar observation was made for some of the pegmatites from Norway
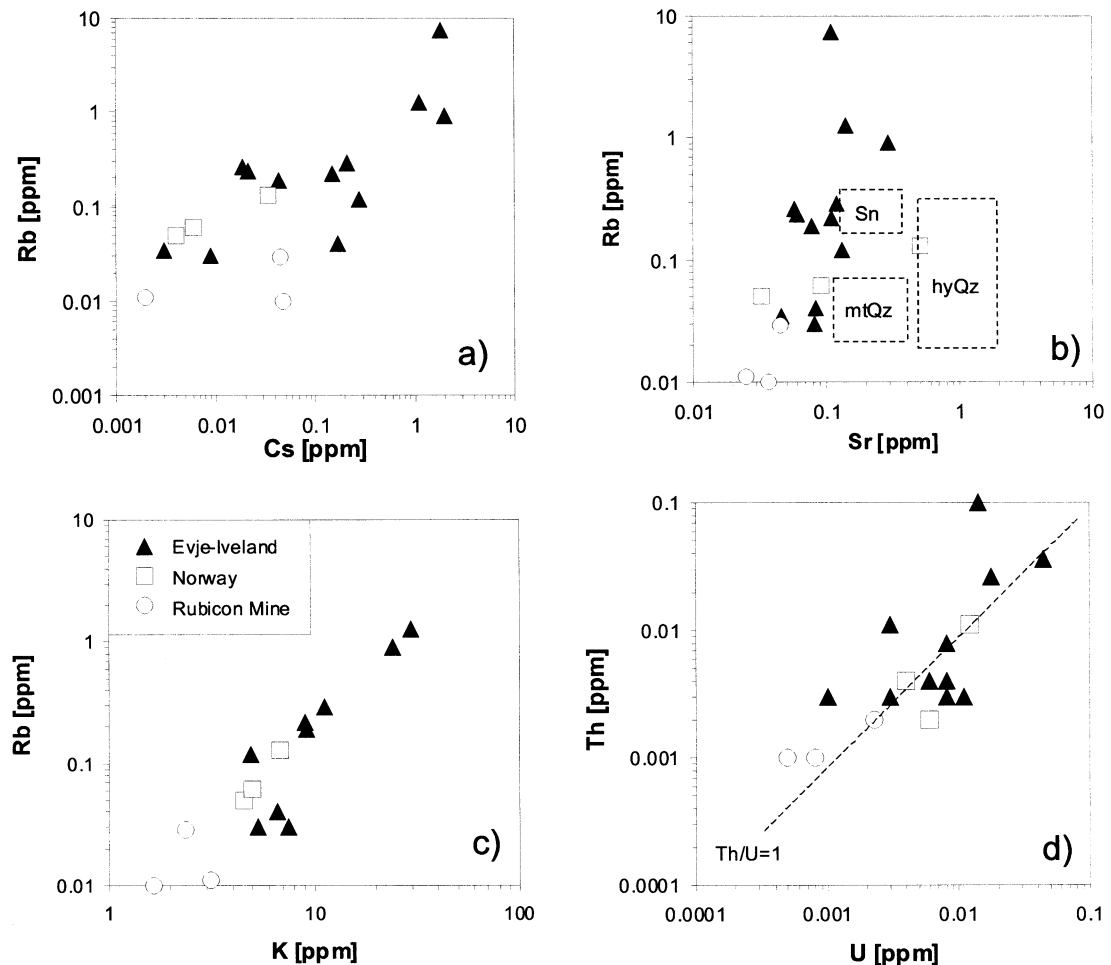
Fig. 2. Selected trace-element correlations of the investigated pegmatite quartz samples. The legend is the same for all diagrams. The fields in the Sr/Rb diagram (b) mark positions for the trace element composition of hydrothermal quartz from Sn deposits (Sn), for metamorphic quartz (mtQz), and hydrothermal quartz from Au deposits (hyQz), after Monecke et al. (2002a).
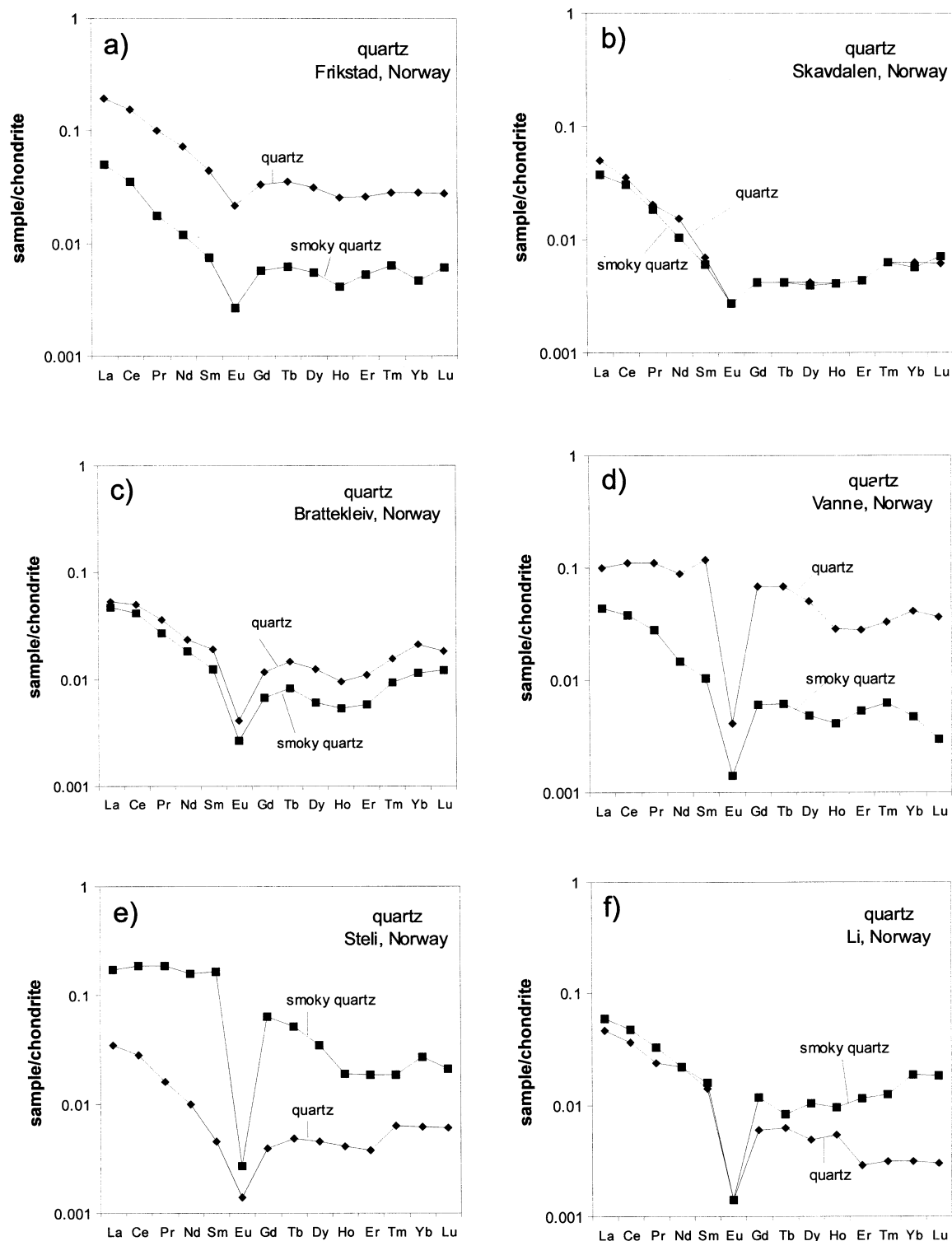
Fig. 3. Chondrite-normalized REE distribution patterns of pegmatite quartz samples from different localities (normal-ization according to data of Mason, 1979). Note that the shape of the REE distribution patterns is almost identical for these sample pairs and do only differ in absolute concentrations.

with Nb/Ta mineralization, which revealed no detectable concentrations of Ta in quartz.

The Rb contents of pegmatite quartz range from 9 to 7360

ppb, which is in the same range as for Cs (Fig. 2a). In contrast, the concentrations of Sr only scatter over a small range (around 0.1 ppm) and are very low in general. The comparison of Rb/Sr
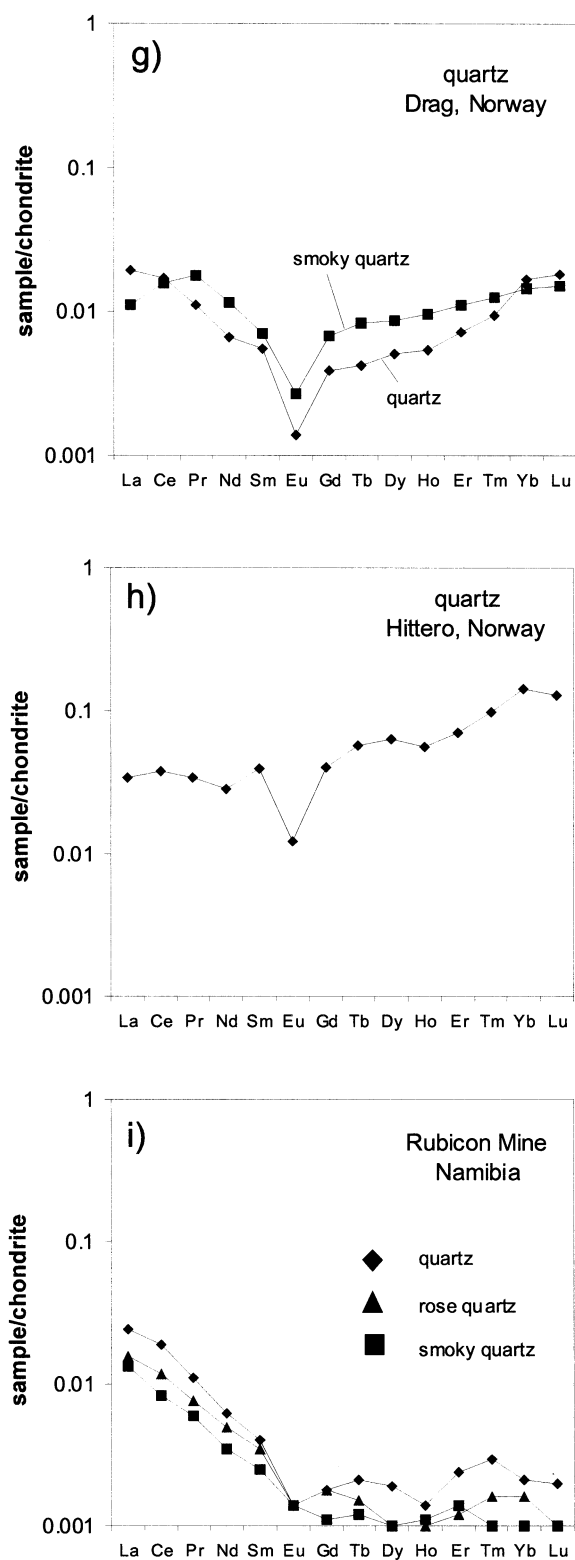
Fig. 3. (Continued)

these results have only preliminary character due to the limited number of samples analyzed. More data points are needed to confirm that this statement is generally valid.

The Th/U ratios of pegmatite quartz significantly differ from the average of 3.8 in the upper continental crust (Taylor and McLennan, 1985). Although the absolute concentrations of both elements are in general below 0.1 ppm, the Th/U ratios are fairly similar and scatter around Th/U = 1 (Fig. 2d).

The chondrite normalized REE patterns show pronounced negative Eu anomalies (Eu/Eu* = 0.03–0.84) and "tetrad effects" (Fig. 3). The term "tetrad effect" refers to the subdivision of the REE series into four groups (four concave-upward segments) that was first reported by Fidelis and Siekierski (1966) and Peppard et al. (1969). The normalized REE concentrations decrease from La to Sm (La_n/Sm_n = 1.1–7.6 with exception of sample Qz9a), whereas the shape of the REE patterns is almost horizontal from Gd to Yb, or slightly increasing (Gd_n/Yb_n = 0.2–2.4). This is especially valid for the samples Qz7a/b from Drag and Qz9a from Hitterø, which show elevated concentrations of the heavy REE (HREE) (La_n/Yb_n of sample Qz9a = 0.3). This phenomenon is probably caused by the primary composition of the mineralizing fluids, which could have been enriched in Y and HREE.

3.2. Electron Spin Resonance

The results of the ESR analysis in this study provide information concerning the abundance and distribution of paramagnetic lattice defects and trace elements, which are incorporated and produce a paramagnetic center in the quartz structure. In general, the pegmatite quartz samples show different center distribution from that of quartz from igneous and metamorphic rocks (Plötze, 1995; Götze and Plötze, 1997). No relationship could be detected between the concentration of paramagnetic centers and coloration of the samples. In all pegmatite quartz samples the following, varied paramagnetic centers were detected (Table 4):

Generally, the abundance of O_2^{3-} centers (silicon vacancy) and E_1' centers (oxygen vacancy) in pegmatite quartz is very low. The $[SiO_3]^{3-}$ center (E'_1 center) consists of an unpaired electron bound on a O^{2-} vacancy (e.g., Weeks, 1956; Weil, 1984). This center could not be detected. The O^- and O_2^{3-} centers represent different types of defect electrons on O^{2-} in tetrahedra with silicon vacancy (e.g., Bershov et al., 1978; Serebrennikov et al., 1982). The low content of lattice defects associated with oxygen or silicon vacancies points to slow growth of quartz crystals from a parental fluid, without supersaturation under constant physicochemical conditions.

The substitutional and interstitial incorporation of trace elements into the quartz lattice resulted, especially, in the formation of paramagnetic centers associated with Al, Ge and Ti. The $[AlO_4]^0$ center was the most intense in the ESR spectra of the quartz samples studied. This center is caused by substitution of Al^{3+} for Si^{4+} with an electron hole trapped by a nonbonding 2p orbital at one of the four nearest O^{2-} ions, forming O^{1-} (Griffiths et al., 1954). The precursor state for this center is the diamagnetic $[AlO_4/M^+]^0$ associated with an adjacent charge compensating cation M^+ (H^+, Li^+, Na^+). During γ-irradiation of quartz at 295 K the M^+-ion may diffuse away yielding the paramagnetic $[AlO_4]^0$ (Nuttall and Weil, 1981). For polycrys-

ratios with data of quartz from other origins (Fig. 2b) illustrates that the pegmatite quartz plots outside the fields for hydrothermal quartz from tin and gold deposits and quartz of metamorphic origin, as reported by Monecke et al. (2002a). However,

Table 4. Results of ESR analysis of quartz samples from different pegmatites (amplitude intensities in arbitrary units).[a]

Sample	Fe^{3+} at g = 4.3 a.u.	signal at g = 2 a.u.	O_2^{3-} at g = 2.005 a.u.	$[GeO_4^-/M^+]^0$ at g = 1.999 a.u.	$[TiO_4^-/Li^+]^0$ at g = 1.913 a.u.	$[AlO_4]^0$ at g = 1.991 a.u.	10^{17} spins/g	ppm
Qz1a	nd	2000	nd	52300	195	27740	2.41	24
Qz1b	50	32000	200	23700	75	27430	2.39	24
Qz2a	nd	11000	nd	3300	110	4740	4.12	4
Qz2b	nd	60000	1000	4800	90	19770	1.72	17
Qz3a	nd	40000	nd	2900	nd	15450	1.34	13
Qz3b	nd	18000	500	8200	75	23480	2.04	20
Qz4a	100	9000	nd	700	8	7440	6.48	6
Qz4b	nd	5000	200	3700	22	13240	1.15	11
Qz5a	nd	37000	200	4700	119	32380	2.82	28
Qz5b	nd	4000	2000	2300	nd	19320	1.68	17
Qz6a	nd	3000	500	1000	35	28800	2.51	25
Qz6b	nd	3500	200	9800	380	41380	3.60	36
Qz7a	nd	4000	500	900	8	32910	2.86	29
Qz7b	nd	4000	nd	500	nd	18780	1.63	16
Qz9a	nd	17000	nd	900	nd	3610	3.14	3
Qz15a	nd	12500	nd	21700	44	15360	1.34	13
Qz15b	nd	19000	500	12800	nd	32810	2.85	28
Qz15c	nd	23000	nd	12000	474	28660	2.49	25

[a] nd = below detection limit.

talline samples the ESR spectrum of $[AlO_4]^0$ exhibits a multi-line spectrum of superimposed 6-line hyperfine patterns (Fig. 4a). The concentration of the Al centers was quantified using a reference sample with known $[AlO_4]^0$ concentration (Moiseev, 1985). This allowed a comparison of the concentration of structurally incorporated Al with the content of bulk trace Al (10^{16} spins/g Al = 1 ppm Al). The results show that the concentration of bulk "trace Al" is higher than structural "ESR Al" (Table 4).

Centers of the type $[TiO_4/Li^+]^0$, which were detected in quartz of the different pegmatites (Table 4), are produced by irradiation of the diamagnetic precursor $[TiO_4]^0$ (Ti^{3+}, i.e., electron center at Ti^{4+}). This precursor is formed by substitution of Ti^{4+} for Si^{4+} at the Si position, where charge compensation is achieved by Li^+ ion at a channel position nearby (Wright et al., 1963; Rinneberg and Weil, 1972). A typical spectrum is shown in Figure 4a.

The Ge-center is of the same type as the Al-center. Substitution of Si^{4+} by Ge^{4+} causes formation of the diamagnetic precursor $[GeO_4]^0$, which transforms to the paramagnetic $[GeO_4]^-$ during γ-irradiation. At room temperature, these centers can bind diffusing M^+ cations, preferentially forming $[GeO_4/Li^+]^0$ and $[GeO_4/H^+]^0$ (Mackey, 1963; Rakov et al., 1985; Weil, 1993). The hyperfine structure is only poorly resolved (Fig. 4b). The probable charge compensation ion might be Li^+ (4 lines at the signal at g = 2.000). Relatively high signal intensities of $[GeO_4/M^+]^0$ centers were found, which corresponds to the elevated concentrations of Ge detected in some of the samples.

Some Fe^{3+} paramagnetic centers may occur in quartz. One of these centers is characterized by substitution of Fe^{3+} for Si^{4+} with charge compensation by alkali ions or protons, so-called S centers $[FeO_4/M^+]^0$ (Stegger and Lehmann, 1989; Mineeva et al., 1991). The signal at g_{eff} 4.3 is characteristic of substitutional Fe^{3+} centers in quartz Figure 4c). The bulk concentration of Fe in the pegmatite quartz samples is very low, and structural Fe^{3+} could only be detected in samples Qz1b and Qz4a (Table 3). The comparison of the Fe^{3+}-center concentration with chemically determined Fe con-

tents does not show any correlation. However, the intense, very broad line at $g_{eff} \sim 2$, which is in general assigned to ferromagnetic inclusions or center clusters with strong spin-spin interaction—usually of transition metal ions (e.g., Fe^{2+}, Fe^{3+})—could be a sign for incorporation of iron into the quartz as center clusters or submicroscopic inclusions.

3.3. Cathodoluminescence (CL) Microscopy and Spectroscopy

The visible CL of all samples is more or less homogeneous bluish-green (Table 1); primary internal structures (e.g., growth zoning) were not found. The CL is caused by two broad emission bands at 505 nm (2.45 eV) and 390 nm (3.18 eV) (Fig. 5). The intensity ratio of these emission bands causes the more bluish or greenish tint of the visible CL color. In most samples the 505 nm band (greenish) dominates the CL emission.

The transient CL disappears after 60–100 s of electron irradiation, and almost no stable component of the emission remains. This transient CL behavior results in a disappearance of the visible CL. The two emission bands show slightly different decay kinetics (Fig. 5). In contrast to hydrothermal quartz, a very weak CL emission band in the red spectral region (650 nm, −1.9 eV) was detected only in a few samples (2a, 4a, 5a, 6a, 7a). This emission was only visible after electron irradiation due to the decreasing intensities of the two dominating emission bands, which covered the red band. Moreover, other characteristic CL emissions occurring in quartz of igneous and hydrothermal origin (e.g., 450 nm, 580 nm), which are associated with lattice defects (oxygen or silicon vacancies), are also lacking.

3.4. Fluid Inclusion Petrography and Microthermometry

Although the analytical techniques used for chemical characterization of the fluid inclusions only allow bulk analysis, different types of inclusions were described by fluid inclusion microscopy and microthermometry. In general, the coarse
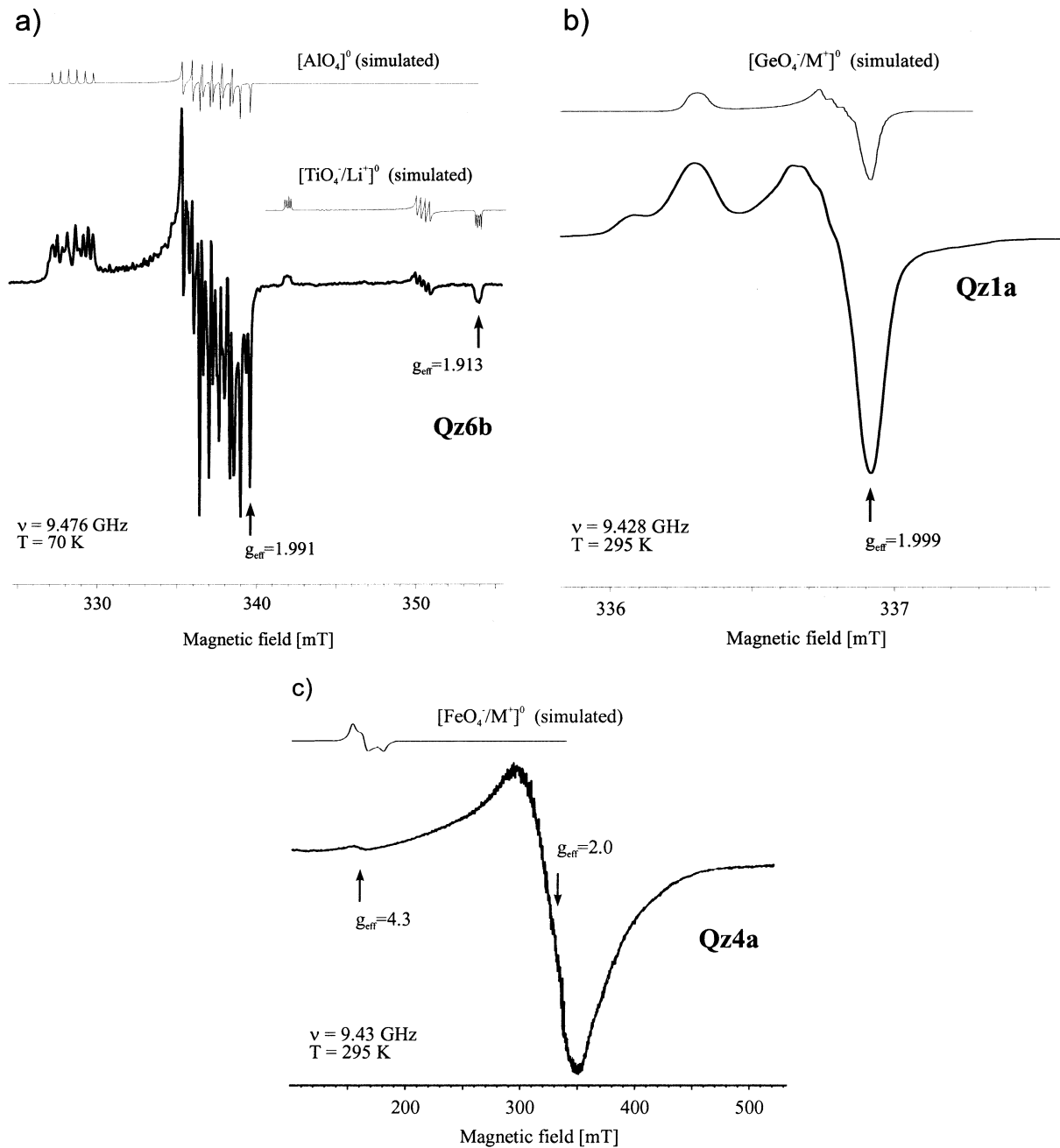
Fig. 4. Selected ESR spectra of trace element centers (a = $[AlO_4]^0$ and $[TiO_4^-/Li^+]^0$; b = $[GeO_4^-/M^+]^0$; c = $[FeO_4^-/M^+]^0$) in pegmatite quartz, in comparison with simulated spectra; arrows mark analytical lines.

quartz grains hosting the fluid inclusion assemblages are only weakly affected by secondary deformation; evidence for significant recrystallization of the mineral could not be observed. The fluid inclusions are classified according to their distribution characteristics in the host quartz samples (Fig. 6) into three types:

Type I inclusions occur as irregular clusters or as groups with no planar orientation. The quartz hosting the inclusions does not show evidence of growth zoning; however, the occurrence of inclusions of Type I in small three-dimensional groups well separated from other inclusions may suggest a primary or early pseudosecondary origin for them (cf. Roedder, 1984). Type II inclusions occur in short trails or in lineations cut by later microstructures. These inclusions could also be pseudosecondary. And Type III inclusions occur in trails cross-cutting older fluid inclusion assemblages and grain boundaries. Inconsistent liquid/vapor-ratios owing to fluid inclusion necking are frequent. These inclusions clearly represent secondary formations.

The pegmatite quartz samples were subdivided into three groups using the fluid inclusion types present and the bulk compositions of the trapped fluids at room temperature.
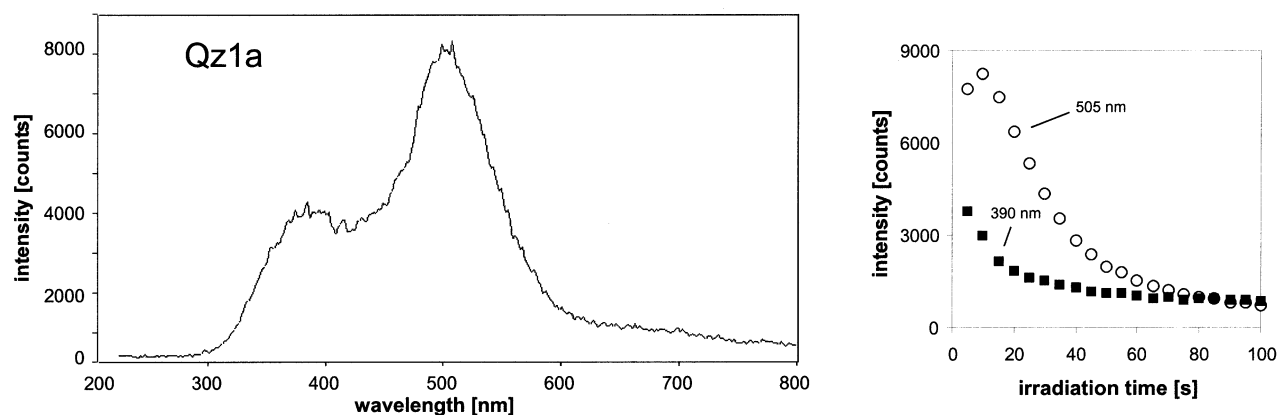
Fig. 5. CL emission spectrum of the quartz sample from Frikstad, Norway showing two main emission bands at 505 nm (2.45 eV) and 390 nm (3.18 eV). The time-dependent behavior of the CL emission during irradiation (right) shows different kinetics for the two main emission bands.

3.4.1. Group 1: Quartz dominated by low-salinity H_2O-CO_2 inclusions

The majority of the samples (most quartz from Evje-Iveland, Norway, and from Rubicon mine, Namibia) belong to a first group that is characterized by a predominance of Type II and III H_2O-CO_2-inclusions. Type I CO_2-bearing inclusions and Type III pure aqueous fluid inclusions were found to occur in subordinate numbers in some of these samples.

H_2O-CO_2-inclusions contain two or three immiscible phases at room temperature in the studied samples. They show predominantly isometric to longish forms. Negative crystal shapes also occur frequently. CO_2-bearing aqueous inclusions mostly have an intermediate degree of fill (F ~ 0.50 to ~ 0.85) and rather homogeneous H_2O/CO_2-rich phase ratios in most inclusions of one group or trail. However, there was a considerable variation in the degree of fill between different samples. Assemblages of Type II CO_2-bearing fluid inclusions showing a very variable degree of filling (F: ~ 0.40 to 0.95) have been found in the quartz sample from Vanne, Evje-Iveland. No leaking or necking down is indicated for these inclusions.

Microthermometric data for H_2O-CO_2-inclusions are summarized in Figure 7. The temperatures of first melting of ice (Tfm) ranged from −27 to −20 °C (Fig. 7a). This indicates a predominance of NaCl as the salt component in the fluid. The temperature of final melting of ice (TmIce) could not be measured for CO_2-bearing inclusions in the investigated samples. Final melting of solid phases always occurred at temperatures above 0°C, which is interpreted to represent the temperature of dissociation of clathrates (TmCLA; Fig. 7b). The measured temperatures of final melting of CO_2 (TmCO_2; Fig. 7c) only show a rather limited variability for all investigated samples. The mostly insignificantly lowered TmCO_2 values indicate the presence of almost pure CO_2 as the nonaqueous volatile (triple point of pure CO_2: −56.6 °C); however, the existence of small amounts of volatiles such as CH_4 and N_2 in the fluid is suggested for the smoky quartz from Vanne by the slightly lower TmCO_2 data (Fig. 7c).

3.4.2. Group 2: Quartz dominated by low-salinity aqueous inclusions

Only pure aqueous inclusions have been trapped in samples of the second group (quartz from Steli and Drak, Norway). Most of them can be clearly identified to belong to the Type III; however, some fluid inclusions occur in short trails.

In general, the pure aqueous inclusions are Type II and III two-phase inclusions at room temperature; however, poorly healed late fluid inclusion trails are often outlined by Type III mono- and two-phase aqueous inclusions showing flat and highly irregular shapes. The Tfm values ranged from −33 to −25 °C in these inclusions (all samples studied; Fig. 7a). This suggests a predominance of NaCl as the salt component in the fluid. The TmIce values were measured in the range from −5.0 to −7.0 °C for inclusions in all investigated samples (Fig. 7b). Final melting of solid phases at temperatures above 0 °C could not be observed for these inclusions.

3.4.3. Group 3: Quartz dominated by brine inclusions

The third group of samples (three samples from Evje-Iveland, Norway) is formed by quartz that is dominated by Type II and, less frequently, Type III multiphase aqueous inclusions. Furthermore, Type III two-phase pure aqueous inclusions with high degrees of fill were observed in the latter group of samples (mono-phase liquid inclusions also occur).

A large number of Type II and III brine inclusions containing one or more daughter minerals was found in three of the investigated samples. The inclusions show isometric to longish forms; negative crystal shapes were also observed. One of the daughter minerals could be identified as NaCl (cubes; isotropic under crossed polars); in addition, tabular crystals often occur. First melting of ice could only be observed for two inclusions. The Tfm values range from −33 to −30 °C (Fig. 7a). The presence of traces of CO_2 in multiphase aqueous inclusions is indicated by final melting of solid phases at temperatures above 0 °C in one of the measured samples (smoky quartz 1b, Frikstadt; Fig. 7b).

In general, a high percentage of the investigated samples is characterized by a predominance of fluid inclusions containing
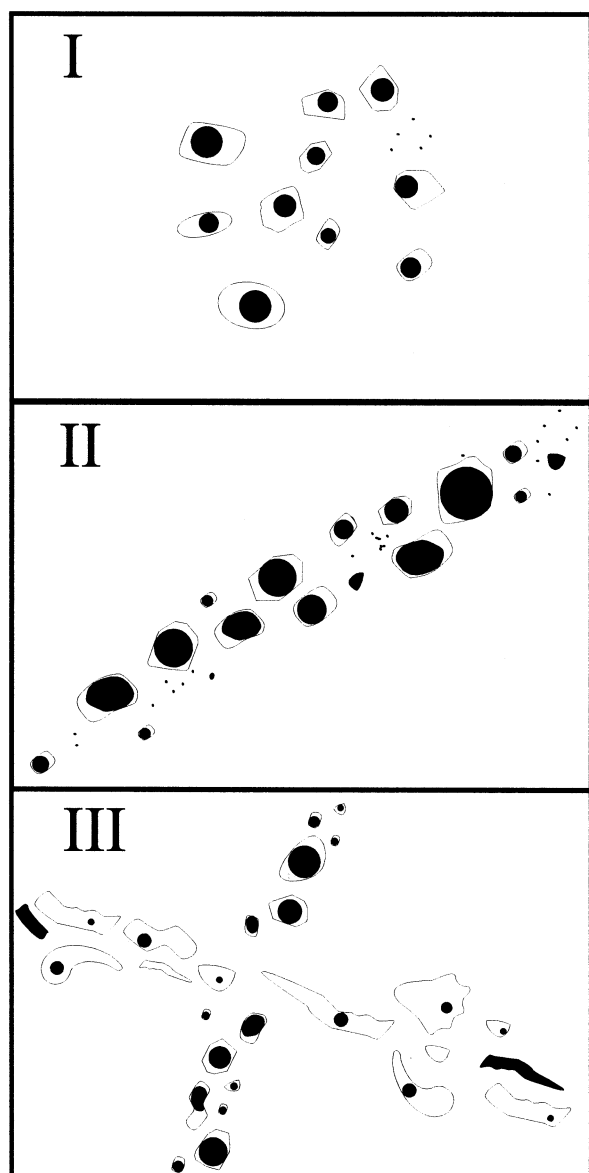
Fig. 6. Main types of fluid inclusions observed in pegmatite quartz of different occurrences. Type I: inclusions occur as irregular clusters or as groups with no planar orientation; Type II: inclusions occur in short trails or in lineations cut by later microstructures; Type III: inclusions occur in trails cross-cutting older fluid inclusion assemblages and grain boundaries; inconsistent L/V-ratios owing to fluid inclusion necking are frequent.

a fluid of a similar composition. In addition to this dominant fluid type, probably late, pure aqueous fluid inclusions occur in variable amounts.

3.5. Fluid Inclusion Bulk Chemistry (Capillary Ion Analysis)

The results of the capillary ion analysis of inclusions in pegmatite quartz (Table 5) show several elements to be present within the fluids. Besides the major elements K, Na, Ca and Mg, trace contents of Li and of the transition metals Co, Ni, Zn,

Pb and Cu were detected in some of the pegmatite quartz samples.

According to their chemical composition, the fluid inclusions in most samples can be classified as H_2O-CO_2-NaCl type inclusions (Table 5, Figs. 8, 9). The Ca, Mg and Li contents are predominantly low. The K/Na ratios in fluid inclusions of the pegmatite quartz samples vary only slightly (0.07–0.33). Furthermore, $NH_4 > K$ was found for all samples except sample Qz15a. Among the anionic complexes, NO_3^-, HCO_3^- and SO_4^{2-} were analyzed in considerable amounts, besides Cl^-. In contrast, F^- seems to play a subordinate role and was only detected in significant amounts in sample Qz1 from Frikstad, Norway. Additionally, the organic ligands acetate and propionate were detected (Table 5). The origin of these organic ligands is unclear (Hallbauer, 1997).

3.6. Bulk Fluid Inclusion Volatile Composition (Gas Chromatography)

The results of the gas chromatographic analysis are summarized in Table 6. Gas analysis shows volatile components in the following order of abundance: $H_2O > CO_2 > N_2(+) \geq CH_4 > COS > C_2$ and C_3 hydrocarbons. Water is the predominant volatile with >90 mol % in most samples. CO_2 concentrations range from < 0.1 to ~ 8 mol % for almost all specimens. Samples Qz2a and Qz15c contain strongly elevated CO_2 contents of 19.7 and 40.8 mol %, respectively. $N_2(+)$ and CH_4 concentrations were always between ~0.02 and 0.8 mol %. The other volatile components are significantly below 0.1 mol percent.

4. DISCUSSION

Although quartz of pegmatitic origin is characterized by low contents of most trace elements (Tables 2 and 3), some elements (e.g., Al, Na, K, Li, Ti, Ge) may be concentrated in remarkable concentrations. The elevated concentrations of K and Na in some samples may suggest the presence of submicroscopic inclusions of muscovite and/or feldspar. However, analyses of the sample material by cathodoluminescence and scanning electron microscopy did not reveal impurities of such minerals. Therefore, we assume that these elements are mostly distributed in the structural channels parallel to the c-axis or bound on aqueous inclusions.

This is confirmed by the correlation of Al versus charge compensating cations in the quartz samples (Fig. 10). There are only a few samples that do not fit along this almost linear correlation. Although the contents of Na and K were above the upper calibration limit of the used analytical method in some samples (Table 2), the high Al contents indicate that they also behave like the other samples.

The results of the ESR measurements revealed that trace Al is indeed incorporated into the quartz structure, as indicated by the good correlation of Al with the compensating alkali ions ($\Sigma Li + Na + K$) (Fig. 10). However, the comparison of the chemically determined trace contents of Al with the contents measured by ESR lacks such good correlation. This is caused by the fact that not all substitutional Al is present in the form of paramagnetic centers. The radiation dose was too low to transform the trace element defects from the nonparamagnetic
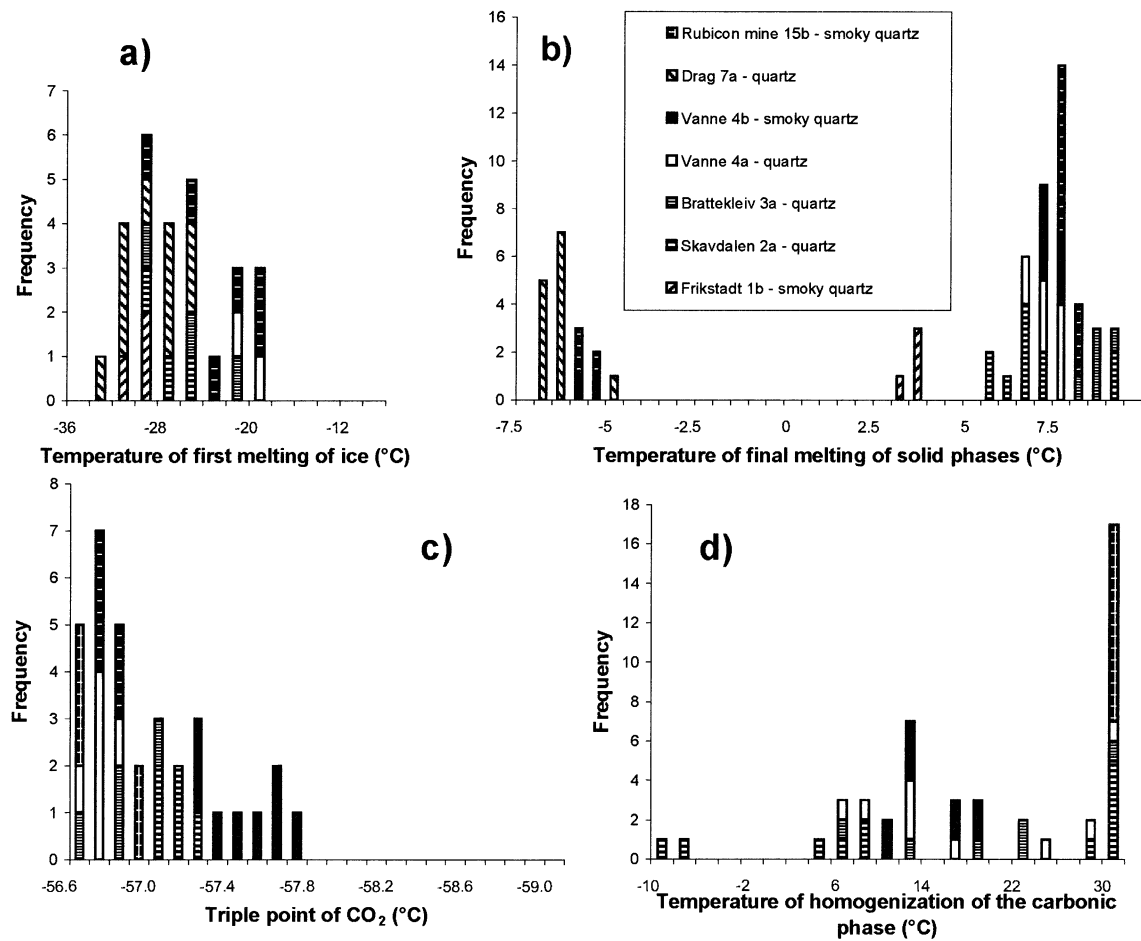
Fig. 7. Diagrams showing the results of the microthermometric investigations on pegmatite quartz samples. (a)Temperature of first melting of ice (*Tfm*); (b) Temperature of final melting of solid phases (temperature of dissociation of clathrates *TmCLA*). (c) Triple point of CO_2 (final melting of CO_2 *TmCO₂*). (d) Temperature of the homogenization of the carbonic phase.

Table 5. Results of capillary ion analysis of fluid inclusions in quartz samples from different pegmatites (all data in mol%).[a]

Sample	NH₄	K	Na	Li	Ca	Mg	Co	Ni	Zn	Pb	Cu	Cl⁻	F⁻	NO₃⁻	HCO₃⁻	SO₄²⁻	Acetate[b]	Propioate[b]
Qz1a	6.45	1.29	9.52	0.17	2.89	0.71	nd	0.44	2.19	nd	1.25	24.75	15.49	8.11	2.75	11.05	0.59	1.08
Qz1b	2.99	1.18	8.06	0.41	1.48	0.42	nd	nd	nd	nd	nd	19.84	3.59	3.63	4.16	3.76	nd	nd
Qz2a	1.63	0.72	9.28	0.22	0.45	0.13	nd	nd	nd	nd	1.08	14.22	1.18	3.00	7.90	2.76	nd	1.71
Qz2b	1.51	0.62	5.03	0.26	0.30	0.09	nd	nd	nd	nd	nd	7.22	—	2.35	7.35	2.53	nd	2.09
Qz3a	1.19	0.33	4.63	—	2.18	0.08	nd	nd	nd	nd	nd	5.72	0.89	2.05	4.05	1.65	0.33	0.18
Qz3b	1.20	0.47	4.74	—	0.49	0.08	nd	nd	nd	nd	nd	9.23	0.35	3.10	4.74	1.42	nd	nd
Qz4a	1.39	1.32	6.94	—	0.47	0.07	nd	nd	nd	nd	nd	10.86	—	1.90	6.90	2.03	nd	nd
Qz4b	1.39	1.07	11.26	0.19	0.64	0.14	nd	nd	nd	nd	nd	19.35	—	3.37	7.75	3.66	nd	nd
Qz5a	0.81	0.52	2.59	—	0.36	0.07	nd	nd	nd	nd	nd	2.69	—	2.25	4.97	1.95	nd	nd
Qz5b	1.08	0.52	4.69	0.12	0.21	0.11	nd	nd	nd	nd	nd	7.30	—	4.52	8.12	2.70	nd	nd
Qz6a	1.02	0.68	5.59	—	0.45	0.08	nd	nd	nd	nd	nd	10.44	—	2.99	4.55	1.45	nd	nd
Qz6b	1.16	0.67	8.31	0.16	0.41	0.11	nd	nd	nd	nd	nd	13.19	—	1.44	8.35	1.38	nd	nd
Qz7a	0.60	0.36	2.42	0.03	0.16	—	nd	nd	nd	nd	nd	1.21	—	1.86	7.16	0.68	nd	nd
Qz7b	1.35	1.04	11.24	0.07	0.38	0.08	nd	nd	nd	nd	nd	9.12	—	2.63	13.52	2.69	nd	nd
Qz9a	1.37	1.20	10.46	0.12	4.15	0.59	nd	nd	nd	nd	nd	25.86	—	1.26	5.08	4.09	nd	0.83
Qz15a	0.96	0.77	2.91	0.19	0.25	0.06	nd	nd	nd	nd	nd	4.62	0.83	2.77	8.14	1.02	nd	nd
Qz15b	0.72	1.16	3.46	—	0.86	0.06	0.09	nd	nd	0.67	nd	6.39	—	6.71	26.47	3.19	nd	nd
Qz15c	1.12	0.54	3.43	0.09	0.42	0.51	nd	nd	nd	nd	0.32	1.54	0.34	1.84	11.81	1.62	1.20	nd

[a] nd = below detection limit (Rb, Sr, Ba, Mn, Br, oxalate, butyrate, WO_4, and HPO_4 were below detection limit in all samples).
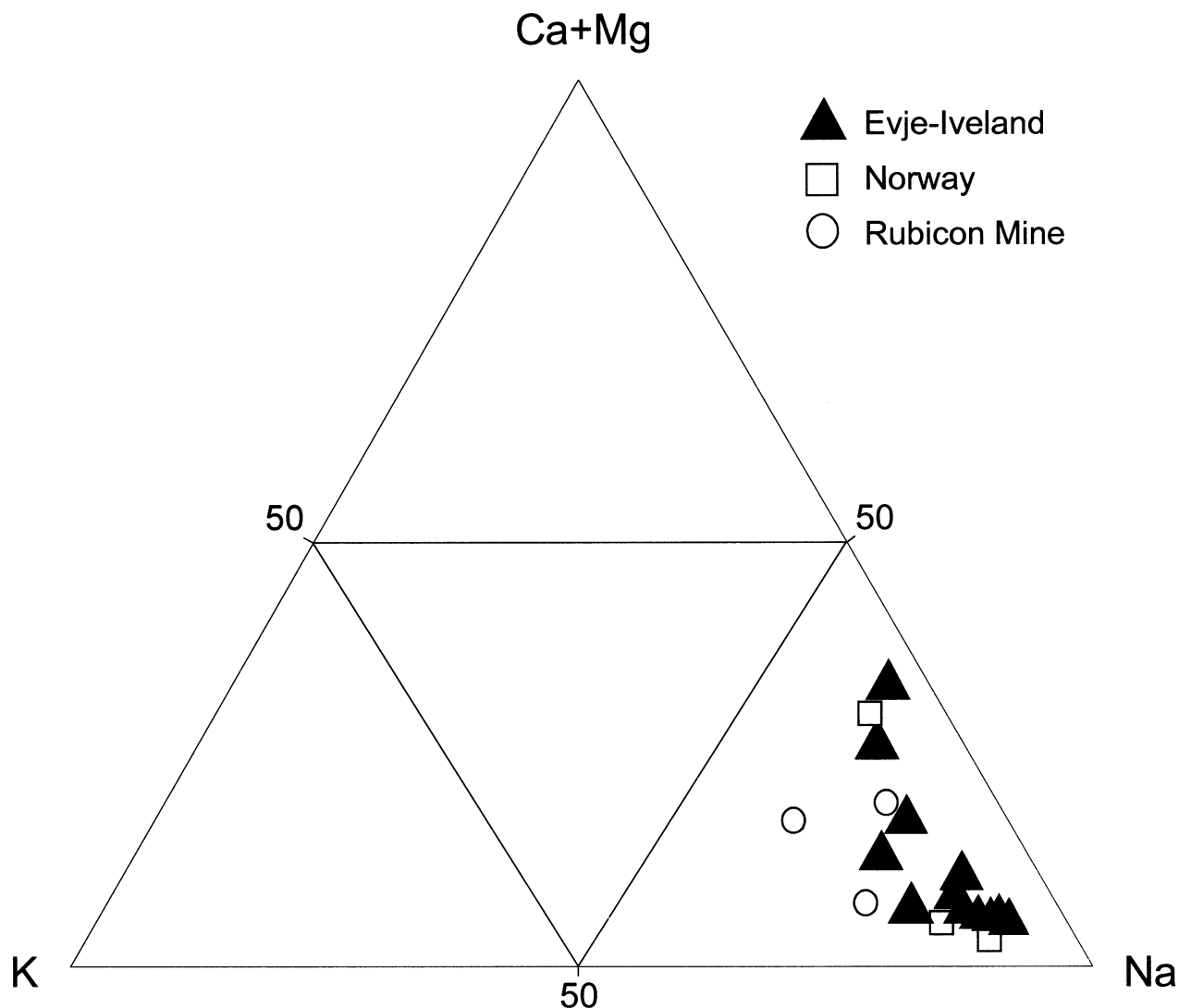[b] Acetate CH_3-COO^-; propionate CH_3-CH_2-COO^-.

Fig. 8. K-Na-(Ca + Mg) diagram for pegmatite quartz samples from different occurrences; the data emphasize the predominance of Na in the inclusion fluids.

precursor state into paramagnetic centers. Al-center saturation is achieved at 1×10^6 Gy. With the applied dose of 1.4×10^4 Gy only ~30% of the Al-defects were transformed into the paramagnetic state (Plötze, 1995). The incomplete conversion of diamagnetic precursors into paramagnetic centers and the existence of diamagnetic defects (e.g., interstitial Al) may be a possible explanation for this phenomenon. On the other hand, there is no evidence from our results that Al is hosted by microinclusions.

Germanium is another trace element that is enriched in pegmatite quartz compared to quartz from other geological settings. The relatively high Ge content may be explained by the higher solubility of GeO_2 in water than SiO_2 at a higher temperature. Therefore, Ge is enriched in late magmatic and hydrothermal fluids (Morey, 1957) and can substitute for Si in the lattice because of the similar ionic radius, which was also reported from agate (Götze et al., 2001a) or hydrothermal quartz (e.g., Schrön et al., 1982; van Moort et al., 1990). The detection of paramagnetic centers of the type $[GeO_4/M^+]^0$ in

quartz of the different pegmatites corresponds to the elevated concentrations of Ge in these samples (Fig. 11). The correlation between "ESR-Ge" and the chemically analyzed bulk Ge contents indicates that the largest part of the Ge is structurally incorporated.

The results of trace element analysis and ESR measurements indicate that the CL emission of pegmatitic quartz can be strongly related to such structural trace-element centers (Götze et al., 2004). Especially the alkali (or hydrogen) compensated centers of Al and Ge ($[AlO_4/M^+]^0$, $[GeO_4/Li^+]^0$) may be responsible for the detected emission bands at 390 and 505 nm, respectively. These transient emissions are sensitive to irradiation damage and can probably be attributed to the recombination of a hole trapped adjacent to a substitutional, charge-compensated center. The rapid attenuation of the CL emission under the electron beam may result from the dissociation and electromigration of the charge compensating cations out of the interaction volume under the influence of the irradiation induced electrical field (Götze et al., 2001b).
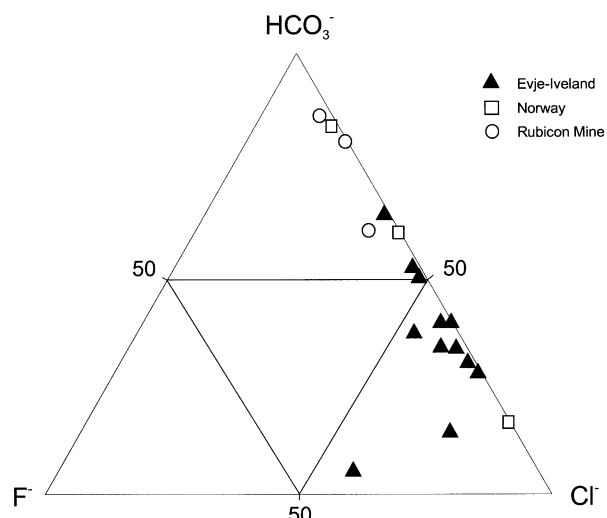
Fig. 9. F^--Cl^--HCO_3^- diagram for pegmatite quartz samples from different occurrences; the inclusion fluids of quartz samples from the Evje-Iveland district, Norway are characterized by high Cl^- contents, whereas the other samples also show significant concentrations of HCO_3^-.
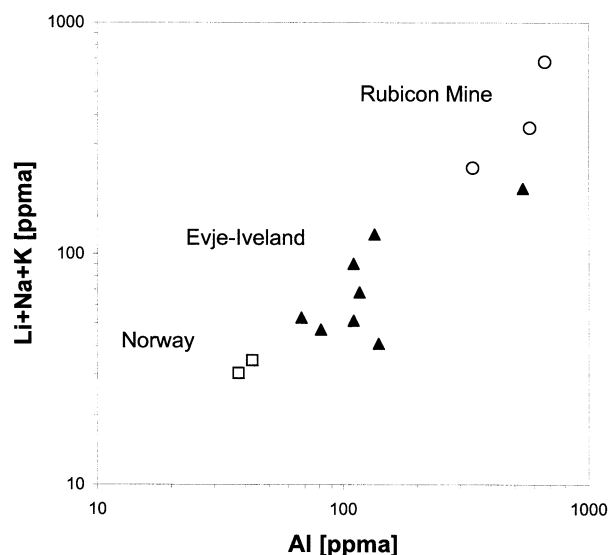

Fig. 10. Correlation of Al versus the sum of charge compensating cations Li + Na + K in the investigated pegmatite quartz samples (the contents are given in ppma = atoms/10^6 atoms Si). The data of samples 2b, 4a, 5b, 6b, and 9a were not plotted into the diagram, as the contents of Na and K, respectively, were above the upper calibration limit of the used analytical method (Table 2).

The comparison of the intensities of the 390 and 505 nm CL emissions with the concentration of trace element centers shows a correlation of the intensity of the 390 nm CL emission with the trace content of Al, whereas the intensity of the 505 nm emission band correlates with the concentration of the $[GeO_4/Li^+]^0$ center (Götze et al., 2004). Because of the varying intensity ratios of the two emission bands in the different quartz samples, we plotted this intensity ratio versus the element ratio Al/Ge (Fig. 12). Although there is no strong linear correlation between these two parameters, the general trend supports our assumption concerning the association of alkali compensated Al and Ge centers with the CL emission bands at 390 and 505

nm, respectively, and would confirm earlier results of Alonso et al. (1983) and Perny et al. (1992). Moreover, CL microscopy revealed a more or less homogeneous distribution of luminescence active trace element centers in the investigated quartz samples. In contrast to most hydrothermal quartz and also some volcanic quartz crystals, where the spatial distribution of Al and compensating cations can vary drastically within one crystal (e.g., Perny et al., 1992; Watt et al., 1997), the pegmatite quartz samples show a homogeneous cathodoluminescence. Only secondary fluid trails were revealed, where the luminescence can

Table 6. Results of gas chromatography of inclusions in quartz samples from different pegmatites[a].

Sample	H_2O	$N_2(+)$	CH_4	CO_2	COS	C_2H_4	$C_2H_6(+)$	C_3H_6	10^{-6} mol H_2O/g quartz
	mo %				ppm (molar)				
Qz1a	99.52	0.03	0.19	0.26	nd	nd	nd	nd	2.33
Qz1b	99.95	0.02	0.04	nd	nd	nd	nd	nd	4.05
Qz2a	80.16	0.09	0.02	19.71	152	1.3	9	nd	16.48
Qz2b	94.23	0.05	0.03	5.68	26	1.0	10	nd	6.69
Qz3a	91.79	0.09	0.27	7.82	176	2.5	45	1.5	4.03
Qz3b	99.69	0.03	0.07	0.21	nd	1.9	27	2.3	4.66
Qz4a	97.39	0.04	0.02	2.54	nd	1.7	20	nd	10.43
Qz4b	95.55	0.08	0.04	4.37	84	1.4	29	0.8	7.99
Qz5a	99.36	0.12	0.22	0.30	nd	nd	nd	nd	0.59
Qz5b	98.96	0.10	0.09	0.84	nd	3.4	42	nd	2.81
Qz6a	97.73	0.03	0.05	2.19	nd	1.1	31	nd	4.27
Qz6b	96.84	0.04	0.02	3.09	nd	1.0	16	nd	8.11
Qz7a	98.45	0.02	0.83	0.69	nd	nd	92	nd	0.67
Qz7b	94.30	0.03	0.04	5.63	11	1.4	22	1.0	11.86
Qz9a	98.40	0.08	0.04	1.48	17	1.3	15	1.0	8.37
Qz15a	97.10	0.03	0.08	2.79	nd	nd	nd	nd	3.17
Qz15b	92.63	0.05	0.11	7.21	nd	nd	nd	nd	2.61
Qz15c	58.54	0.31	0.25	40.81	911	nd	73	5.1	1.22

[a] nd = below detection limit (C_3H_4 and C_3H_8 were below detection limit in all samples). $N_2(+)$ and $C_2H_6(+)$ mean that N_2 ($\pm CO$; $\pm Ar$; $\pm O_2$) and C_2H_6 ($\pm C_2H_2$) are maximum concentrations.
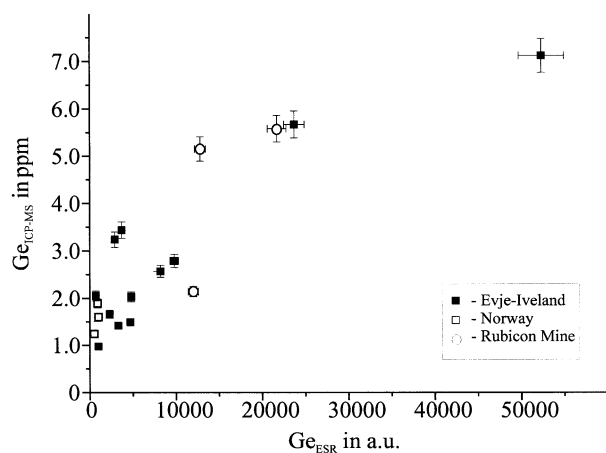
Fig. 11. Plot of bulk Ge content in pegmatite quartz analyzed by ICP-MS versus concentration of structurally incorporated Ge determined as paramagnetic $[GeO_4/M^+]^0$ centers by ESR measurements.

Fig. 13. Plot of bulk Ti content in pegmatite quartz analyzed by ICP-MS versus concentration of structurally incorporated Ti determined as paramagnetic $[TiO_4/Li^+]^0$ centers by ESR measurements (the error bar for low concentrations is in the range of the symbol size). Only for the quartz samples from the Rubicon Mine, Namibia (circles), the data show a linear correlation with zero intercept that indicates a complete presence of Ti as structural substituent for Si. All other samples have, at least partly, a contribution of Ti from mineral microinclusions (e.g., rutile).

be enhanced or quenched by the redistribution of such luminescence active elements or recrystallization processes during the migration of fluids through the quartz lattice (Van den Kerkhof and Hein, 2001).

Paramagnetic centers of the type $[TiO_4/Li^+]^0$ were also detected in quartz of the different pegmatites and evidenced the structural incorporation of Ti into the quartz lattice. However, the comparison of Ti center concentration versus bulk Ti content in all quartz samples in Figure 13 reveals that in most samples these values do not correlate. Three types of quartz samples may be distinguished: (1) The quartz samples from the Rubicon Mine (Qz 15a,b,c) show a perfect linear correlation with zero intercept on the Ti axis indicating a complete structural incorporation of Ti into the quartz lattice. Interestingly, the rose quartz sample (Qz15c) shows the highest concentration of structurally incorporated Ti. Although Goreva et al. (2001) proposed that the rose color in quartz is caused by the occur-

rence of dumortierite-like microfibers, the recent results indicate the role of structural Ti as source for the color in rose quartz, as earlier suggested by Wright et al. (1963). (2) Quartz from the pegmatites of Drag (Qz7a/b) and Hitterø (Qz9a), Norway have Ti contents between 2.05 and 8.68 ppm without measurable structural Ti. We interpret this as resulting from the occurrence of Ti exclusively in mineral micro-inclusions (rutile). (3) The third group includes most of the pegmatite quartz from the Evje-Iveland district. In these samples both types of Ti occurrence exist. Increasing amounts of structural Ti may, in general, cause increasing bulk Ti contents, but a general apparent nonzero intercept on the Ti axis indicates the occurrence of nonstructurally incorporated Ti. A lack of correlation in samples with high Ti contents may be due to rutile inclusions. The height over the line, as defined by the samples Qz 15a,b,c in Figure 13, gives an indication of the amount of titanium that is not structurally bound in quartz.

The presence of rutile inclusions in quartz may be explained by the temperature dependence of the trace-element incorporation. Because of its ionic radius, Ti^{4+} is in general sixfold coordinated by O^{2-}. Only at elevated temperatures titanium can substitute as Ti^{4+} in fourfold coordination for Si^{4+} resulting in exsolution of TiO_2 during cooling (Blankenburg et al., 1994). Therefore, rutile microinclusions in magmatic quartz may be frequent.

A different behavior is also observed for the alkali elements in quartz, which may be both structurally incorporated on interstitial positions in the quartz lattice and hosted in fluid inclusions. The results of the ESR measurements show that there may be a redistribution of interstitial alkali ions in the quartz lattice during irradiation. The diamagnetic $[AlO_4/M^+]$ center transforms into the paramagnetic $[AlO_4]^0$ center, whereas the compensating ions diffuse away under the influence of irradiation. In contrast, the diamagnetic precursor centers of $[TiO_4]^0$ and $[GeO_4]^0$ may capture an electron and
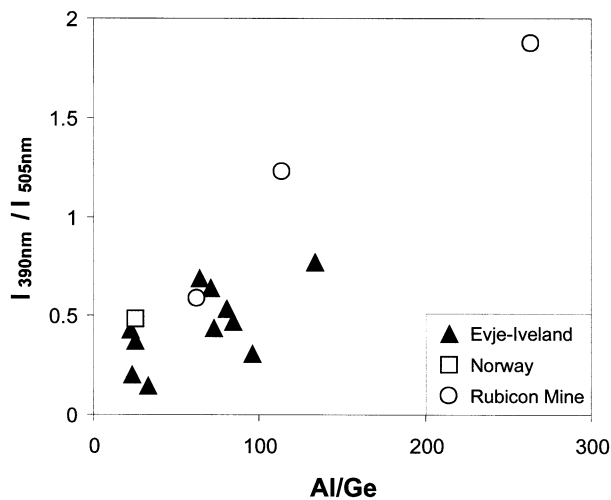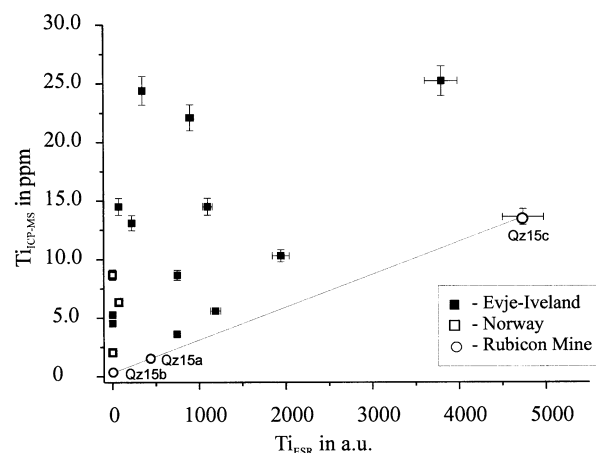

Fig. 12. Plot of the ratio of the CL emission intensities of the 390 and 505 nm emission bands, respectively, versus the ratio of the trace element contents of Al and Ge (symbols as in Fig. 1).
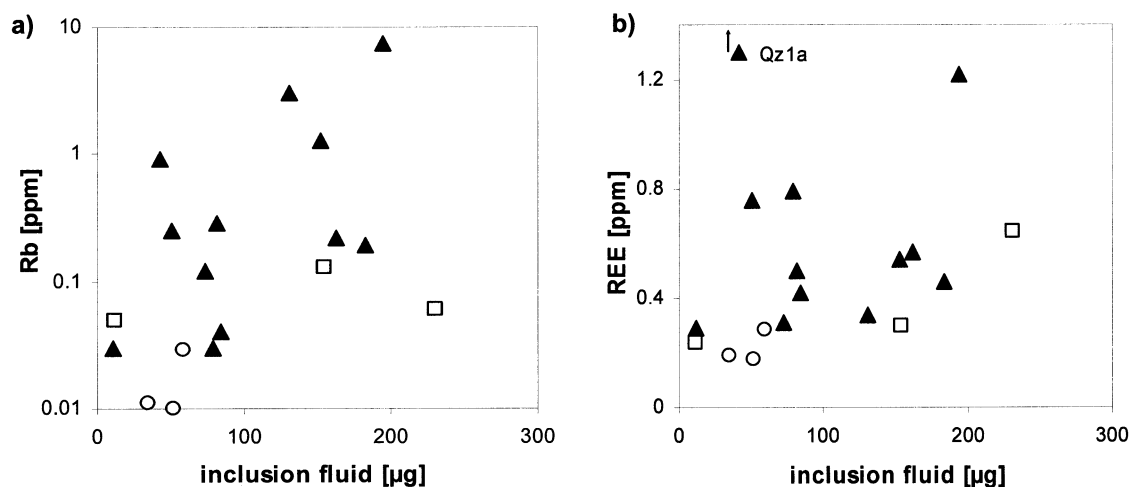
Fig. 14. Plots of Rb (a) and ΣREE (b) versus total amount of inclusion fluids in investigated pegmatite quartz samples (symbols as in Fig. 1). The diagrams show a general trend of increasing Rb and REE contents, respectively, with increasing amount of inclusion fluid, indicating that these elements are preferentially hosted by fluid inclusions in quartz. The scatter may be explained by different absolute concentrations of these elements in the inclusion fluids of the individual samples.

diffusing ions for charge compensating, and form paramagnetic centers. This is the reason why some of the sample pairs from single deposits (e.g., samples Qz1, Qz3, Qz15) show good correlations between bulk element contents and concentrations analyzed by ESR, whereas others do not. In the latter case, the Li content is probably not sufficient to compensate all Ti-related defects and to convert all diamagnetic precursors.

The bulk concentration of Fe in the pegmatite quartz samples is very low and hardly any structural Fe^{3+} could be detected. This finding is in good agreement with the characteristic high Ge/Fe ratio (4.5–0.1) of quartz from pegmatites, compared to quartz samples of other origin.

In general, the contribution of the fluid inclusions to the bulk trace element composition may be estimated by using the volatile content of the quartz samples. The results illustrate that some trace elements in quartz (in particular K, Na, Ca and Mg) can be concentrated in fluid inclusions at the ppm level. In conclusion, not all Na and K may act as charge balancing cations for Al, as indicated from the correlation in Figure 10. Several ppm of Na + K may also be hosted by fluid inclusions. Interestingly, the Li concentrations in fluid inclusions are generally very low, even in the quartz samples from Li pegmatites; the bulk Li content in quartz may reach more than hundred ppm. In contrast to the other alkali elements, Li seems to be exclusively incorporated into the structural channels of the quartz lattice as charge balancing cation for Al, Ge and Ti. This result confirms previous suggestions of Stavrov et al. (1978), who proposed a dominant role of Li as charge balancing cation for Al in granite and pegmatite quartz, compared to the other alkali earths Na, K, Rb and Cs.

K and Rb show in general a similar geochemical behavior (Fig. 2), but the K/Rb ratio is not constant for quartz and ranges over an order of magnitude for the investigated samples (~200 for low Rb contents, and ~20 for high Rb concentrations). Thus, Rb must be treated as an individual element and not as an element "camouflaged" by potassium, a fact that was already reported for feldspar minerals by Smith (1983). This may emphasize the conclusion of Rossman et al. (1987) and Mon-

ecke et al. (2002) that rubidium is mainly hosted in fluid inclusions in quartz although we could not directly analyze it. The correlation of Rb versus the fluid content (Fig. 14a) illustrates the general trend of increasing Rb contents with increasing amounts of inclusion fluid.

Other studies have revealed that fluid inclusions may host a wide range of other elements (e.g., Malinko et al., 1976; Hallbauer and Kable, 1982; Gerler and Schnier, 1989; Gerler, 1990; Channer and Spooner, 1992; Yardley et al., 1993). Results of Rossman et al. (1987), Ghazi et al. (1993) and Monecke et al. (2002) suggested that besides Rb and Sr, also the lanthanides are preferentially hosted by the fluid inclusions. Although the concentrations of these elements could not directly be analyzed in the present study, there are some indications which support these conclusions.

The sample pairs (quartz-smoky quartz) in each of the deposits show more or less identical chondrite-normalized REE distribution patterns; however, the absolute concentrations are different in some cases (e.g., samples Qz1, Qz4, Qz5). Assuming that the REEs are preferentially bound in fluid inclusions, these differences may be explained by varying abundance of aqueous inclusions in the quartz samples. Although the absolute concentrations of REE in the inclusion fluids are too low to be quantified by capillary ion analysis, the results of SEM studies and GC measurements support this hypothesis. In samples with high concentrations of ΣREE, the content of fluid inclusions and the absolute water content of the samples was higher than in those with low ΣREE contents (Fig. 14b). These results may emphasize the role of fluid inclusions in hosting REE in quartz. Consequently, the REE contents in quartz may reflect the chemistry of mineral-forming fluids.

Despite some differences in the chondrite-normalized REE distribution, most samples show similar patterns with pronounced negative Eu anomalies (Eu/Eu* 0.03–0.84) and "tetrad effects" (Fig. 3). Recent results of Monecke et al. (2002b) showed that the convex tetrad effect in samples from magmatic environments can most likely be explained by formation within the magma-fluid system before emplacement in the subvolcanic

environment, where phase separation causes a split of this system into fluid and magma subsystems. The negative Eu anomaly is also assumed to be a characteristic feature of late magmatic fluids (especially in evolved granitic systems), although there is no relationship between the intensity of the Eu anomaly and the development of tetrad effects (Monecke et al., 2002b).

For a number of elements the "type" of incorporation in quartz could not directly be determined. These are especially those elements that are present in extremely low concentrations (e.g., U, Th, Nb, Ta, Cs) in quartz. We conclude that these ions are either too large to substitute for the small Si^{4+} ion (0.42Å) or that they are not soluble in the mineralizing solutions to be incorporated in fluid inclusions. Schrön et al. (1988b) concluded that elements such as Be, Nb or Ta are mainly mobile as gaseous chloro- or fluoro-complexes, because of their low solubility in aqueous solutions. Probably, traces of these elements are situated on interstitial places in the lattice or bound on submicroscopic mineral inclusions (e.g., on grain boundaries) that were not detectable during sample preparation.

Some elements, which are concentrated in the specific mineralization of certain pegmatites, are not present in elevated concentrations in the paragenetic pegmatite quartz itself. This was observed, for instance, for the elements Be, Cs and Rb in the Li (Be-Cs-Rb) pegmatites of Rubicon or for Nb and Ta for Nb-Ta bearing pegmatites from Norway. Because of the partitioning effects during crystallization, the concentration of these trace elements in quartz does not reflect the mineralization and, thus, cannot be used as petrogenetic indicator.

5. CONCLUSIONS

Trace elements in minerals are important petrogenetic indicators in geosciences. In the present study pegmatite quartz from different geological settings was analyzed to obtain information on the general trace element composition and the different mechanisms of incorporation of certain elements. For this reason, an analytical combination of ICP-MS, Capillary Ion Analysis (CIA), Gas Chromatography (GC) and Electron Spin Resonance (ESR) was chosen. Each of these analytical techniques provided specific information about the trace element uptake in quartz. Because of the very low concentrations of most elements in quartz, special emphasis was placed on careful sample selection and preparation. Therefore, the investigations were accompanied by light and cathodoluminescence microscopy, fluid inclusion studies and scanning electron microscopy.

In general, the pegmatite quartz samples show similar geochemical characteristics with low contents of most trace elements. Only the elements Al, Ti, Ge, Na, K, and Li have appreciable concentrations in quartz. The results of the ESR studies, as well as the linear correlation of Al with the charge compensating cations Li, Na and K, revealed that these elements are preferentially incorporated on the Si position (Al, Ti, Ge) or in structural channels parallel to the c-axis (Li, Na, K) in the quartz lattice. Whereas Li is almost exclusively structurally incorporated and plays the most important role in compensating Al in the quartz structure, some ppm of Na and K may also be hosted by fluid inclusions. Ti may both be incorporated as substitutional ion for Si and bound on mineral microinclu-

sions (rutile). In different samples varying proportions of these two types of trace element input were detected.

Considerable amounts of Na, K, NH_4, Ca and Mg can be hosted in fluid inclusions in pegmatite quartz. Additionally, traces of the metals Co, Ni, Zn, Pb, and Cu were detected by CIA in fluid inclusions of some samples. Furthermore, there are indications that the REE and Rb are also bound in fluid inclusions, but the concentrations of these elements are too low to be measured by CIA. According to their chemical composition, the fluid inclusions in pegmatite quartz can, in general, be classified as H_2O-CO_2-NaCl type inclusions, with water as the predominant volatile. Among the anionic complexes, Cl^-, NO_3^-, HCO_3^- and SO_4^{2-} were detected.

For a number of elements the "type" of incorporation in quartz could not directly be determined. Because of their extremely low concentrations, the position of these elements in the quartz lattice could not be revealed by the analytical techniques used. Other sophisticated techniques (e.g., ICP-MS of inclusion fluids) have to be further developed to provide more detailed information (e.g., Ghazi et al., 1993).

For genetic interpretations it has to be concluded that different trace elements in quartz behave in very contrasting ways. Elements such as Al, Ge, Li, REE or element ratios of Ge/Fe or Th/U seem to be reliable indicators of specific geological settings. Concentrations of other elements (e.g., Be, Cs, Nb, Ta) do not reflect the specific mineralization and, thus, cannot be used as petrogenetic indicators. This fact has to be considered if trace elements in quartz should be used as pathfinder elements for geochemical processes.

REFERENCES

Alonso P. J., Halliburton L. E., Kohnke E. E., and Bossoli R. B. (1983) X-ray induced luminescence in crystalline SiO_2. *J. Appl. Phys.* **54,** 5369–5375.

Bambauer H. U. (1961) Spurenelemente und γ-Farbzentren in Quarzen aus Zerrklüften der Schweizer Alpen. *Schweiz. Min. Petrogr. Mitt.* **41,** 335–367.

Baranova N. N., Kozerenko S. V., Grigorian S. S., Daryna T. G., and Saveljev B. V. (1980) Experimental results about concentrations of gold and silver in hydrothermal solutions (in Russian). *Geokhimiya* **8,** 146–157.

Bershov L. V., Marfunin A. S., and Speranskij A. V. (1978) A new stable radiogenic center in quartz (in Russian). *Izv. AN SSSR, ser. Geol.* **11,** 106–116.

Bjørlykke K. (1934) The mineral paragenesis and classification of the granite pegmatites of Iveland, Satesdal, South Norway. *Norsk Geologisk Tidsskrift.* **14,** 211–311.

Blankenburg H.-J., Götze J., Schulz H. (1994) *Quarzrohstoffe.* Deutscher Verlag für Grundstoffindustrie.

Bottrell S. H., Yardley B. W. D., and Buckley F. (1988) A modified crush-leach method for the analysis of fluid inclusion electrolytes. *Bull. Miner.* **111,** 279–290.

Bray C. J., Spooner E. T. C., and Thomas A. V. (1991) Fluid inclusion volatile analysis by heated crushing, on line gas chromatography: Applications to Archean fluids. *J. Geochem. Explor.* **42,** 167–193.

Channer D. M. DeR. and Spooner E. T. C. (1992) Combined gas and ion chromatographic analysis of fluid inclusions from quartz and determination of Cl-Br-I ratios in trapped fluids. In *Program and Abstracts of the Pan-American Conference on Research on Fluid Inclusions,* 4:21. University of California.

Channer D. M., DeR., Bray C. J., and Spooner E. T. C. (1999) Integrated cation-anion/volatile fluid inclusion analysis by gas and ion chromatography; methodology and examples. *Chem. Geol.* **154,** 59–82.

Czamanske G. K., Roedder E., and Burns F. (1963) Neutron activation analysis of fluid inclusions for copper, manganese, and zinc. *Science* **140,** 401–403.

Dennen W. H. (1964) Impurities in quartz. *Geol. Soc. Am. Bull.* **75,** 241–246.

Dennen W. H. (1966) Stochiometric substitution in natural quartz. *Geoch. Cosm. Acta* **30,** 1235–1241.

Dennen W. H. (1967) Trace elements in quartz as indicators of provenance. *Geol. Soc. Am. Bull.* **78,** 125–130.

Fidelis I. and Siekierski S. (1966) The regularities in stability constants of some rare earth complexes. *J. Inorg. Nucl. Chem.* **28,** 185–188.

Gerler J. (1990) Geochemische Untersuchungen an hydrothermalen, metamorphen, granitischen und pegmatitischen Quarzen und deren Flüssigkeitseinschlüssen. PhD thesis. University Göttingen.

Gerler J. and Schnier C. (1989) Neutron activation analysis of liquid inclusions exemplified by a quartz sample from the Ramsbeck Mine, FRG. *Nucl. Geophys.* **3,** 41–48.

Ghazi A. M., Vanko D. A., Roedder E., and Seeley R. C. (1993) Determination of rare earth elements in fluid inclusions by inductively coupled plasma-mass spectrometry (ICP-MS). *Geochim. Cosmochim. Acta* **57,** 4513–4516.

Goreva J. S., Ma Ch., and Rossman G. R. (2001) Fibrous nanoinclusions in massive rose quartz: The origin of rose coloration. *Am. Mineral.* **86,** 466–472.

Götze J. and Lewis R. (1994) Distribution of REE and trace elements in size and mineral fractions of high purity quartz sands. *Chem. Geol.* **114,** 43–57.

Götze J. and Plötze M. (1997) Investigation of trace-element distribution in detrital quartz by Electron Paramagnetic Resonance (EPR). *Eur. J. Miner.* **9,** 529–537.

Götze J. and Zimmerle W. (2000) Quartz and silica as guide to provenance in sediments and sedimentary rocks. In *Contrib. Sed. Geol.*21. Schweizerbart-sche Verlagsbuchh. Nägele & Obermiller Stuttgart. 91 pp.

Götze J., Tichomirowa M., Fuchs H., Pilot J., and Sharp Z. D. (2001a) Geochemistry of agates: A trace element and stable isotope study. *Chem. Geol.* **175,** 523–541.

Götze J., Plötze M., and Habermann D. (2001b) Origin, characteristics and practical applications of the cathodoluminescence (CL) of quartz: A review. *Mineral. Petrol* **71,** 225–250.

Götze J., Plötze M., and Trautmann T. (2004) Structure and luminescence characteristics of quartz from pegmatites. *Amer. Mineral.* (in press).

Griffiths J. H. E., Owen J., and Ward I. M. (1954) Paramagnetic resonance in neutron-irradiated diamond and smoky quartz. *Nature* **173,** 439–442.

Hallbauer D. K. (1992) The use of selected trace elements in vein quartz and quartz pebbles in identifying processes of formation and source rocks (abstract). In *Geol. Soc. South Africa 24th Congress, Bloemfontein,*157–159.

Hallbauer D. K. (1997) The application of capillary ion analysis to the geochemistry of natural aqueous fluids and in particular to the analysis of fluid inclusions in minerals. *Proc. 30th Int. Geol. Congr.* **9,** 409–424.

Hallbauer D. K. and Kable E. J. D. (1982) Fluid inclusions and trace element content of quartz and pyrite pebbles from Witwatersrand conglomerates; their significance with respect to the genesis of primary deposits. In *Orogenesis: The State of the Art* (eds. Amstutz et al.), pp. 742–752. Springer-Verlag.

Heynke U., Leeder O., and Schulz H. (1992) On distinguishing quartz of hydrothermal or metamorphogenic origin in different monomineralic veins in the eastern part of Germany. *Miner. Petrol* **46,** 315–329.

Jandik P. and Bonn G. (1993) *Capillary Electrophoresis of Small Molecules and Ions.* VCH Publishers.

Jung L., ed. (1992) *High Purity Natural Quartz. Part I: High Purity Natural Quartz for Industrial Use. Part II: High Purity Natural Quartz Markets for Suppliers and Users.* Quartz Technology.

Keller P. (1999) Herkunft, Fraktionierung und Mineralisation der Pegmatite des Karibib-Belts, Namibia. *Eur. J. Mineral* **11,** 120.

Klemm W. (1994) Chemical evolution of hydrothermal solutions during Variscan and post-Variscan mineralization in the Erzgebirge, Germany. In *Metallogeny of Collosional Orogens* (eds. R. Seltmann, H. Kämpf and P. Möller), pp. 150–;158. Czech Geological Survey.

Larsen R. B. (2002) The distribution of rare-earth elements in K-feldspar as an indicator of petrogenetic processes in granitic pegmatites: Examples from two pegmatite fields in southern Norway. *Can. Mineral* **40,** 137–151.

Larsen R. B., Polvé M., and Juve G. (2000) Granite pegmatite quartz from Evje-Iveland: Trace element chemistry and implications for high-purity quartz formation. *Norges Geologiske Undersøkelse Bulletin* **436,** 57–65.

Lyakhovich V. V. (1972) Trace Elements in Rock-Forming Minerals of Granitoides (in Russian). Izd. Nedra, Moscow, 200 pp.

Malinko S. V., Berman I. B., Rudnev V. V., and Stolyarova A. N. (1976) Inclusions of boron-bearing hydrothermal solutions in quartz crystals based on (n, α) radiography (in Russian). *Dokl. Akad. Nauk SSSR* **228,** 117–120.

Mason B. (1979) Cosmochemistry, Part I. Meteorites. In *Data of Geochemistry* (ed. M. Fleischer). Professional Paper 440-B1. U.S. Geological Survey.

Mackey J. H. (1963) EPR study of impurity-related color centers in germanium-doped quartz. *J. Chem. Phys.* **39,** 74–83.

Mineeva RM., Bershov LV., and Petrov I. (1991) EPR of surface-bound Fe^{3+} ions in polycrystalline quartz (in Russian). *Dokl. AN SSSR.* **321,** 368–372.

Moiseev B. M. (1985) Natural Radiation Processes in Minerals. Izd. Nedra, Russian, in.

Monecke T., Kempe U., Petersen S., Götze J., Herzig P. and Wolf D. (1999) Trace element characteristics of quartz from the TAG hydrothermal mound (Mid-Atlantic Ridge at 26E08′N). In *Mineral Deposits: Processes to Processing,* pp. 551–554. Balkema.

Monecke T., Bombach G., Klemm W., Kempe U., Götze J., and Wolf D. (2000) Determination of trace elements in the quartz reference material UNS-SpS and in natural quartz samples by ICP-MS. *Geostand. Newsl.* **24,** 73–81.

Monecke T., Kempe U., and Götze J. (2002a) Genetic significance of the trace element content in metamorphic and hydrothermal quartz: A reconnaissance study. *Earth Planet. Sci. Lett.* **202,** 709–724.

Monecke T., Kempe U., Monecke J., Sala M., and Wolf D. (2002b) Tetrad effect in rare earth element distribution patterns: A method of quantification with application to rock and mineral samples from granite-related rare metal deposits. *Geochim. Cosmochim. Acta* **66,** 1185–1.

Morey G. W. (1957) The solubility of solids in gasses. *Econ. Geol.* **52,** 225–251.

Müller A., Wiedenbeck M., Van den Kerkhof A. M., Kronz A., and Simon K. (2003) Trace elements in quartz—A combined electron microprobe, secondary ion mass spectrometry, laser-ablation ICP-MS, and cathodoluminescence study. *Eur. J. Miner.* **15,** 747–763.

Naumov G. B., Mironova O. F., Saveleva N. I., and Danilova T. V. (1984) Concentration of uranium in hydrothermal solutions obtained from investigations of fluid inclusions (in Russ.). *Dokl. Akad. Nauk SSSR* **279,** 1486–1488.

Nettar D. and Villafranca J. J. (1985) A programm for EPR powder spectra simulation. *J. Magn. Res.* **64,** 61.

Nuttall R. H. D. and Weil J. A. (1981) The magnetic properties of the oxygen-hole aluminium centers in crystalline SiO_2. I. $[AlO_4]^0$. *Can. J. Phys.* **59,** 1696–1708.

Oftedahl Ch. (1980) Geology of Norway. *Norges Geol. Undersøkelse Bull.* **357,** 1–114.

Pedersen S. (1981) Rb/Sr age determinations on the late Proterozoic granitoids from the Evje area, South Norway. *Bull. Geol. Soc. Denmark* **29,** 129–143.

Peppard D. F., Mason G. W., and Lewey S. (1969) A tetrad effect in the liquid-liquid extraction ordering of lanthanide(III). *J. Inorg. Nucl. Chem.* **31,** 2271–2272.

Perny B., Eberhardt P., Ramseyer K., Mullis J., and Pankrath R. (1992) Microdistribution of Al, Li, and Na in α-quartz: Possible causes and correlation with short-lived cathodoluminescence. *Am. Miner.* **77,** 534–544.

Pickney D. M. and Haffty J. (1970) Content of zinc and copper in some fluid inclusions from the Cave-in-Rock district, South Illinois. *Econ. Geol.* **65,** 451–458.

Plötze M. (1995) EPR-Untersuchungen an Quarz, Scheelit und Fluorit aus hochthermalen Seltenmetallvererzungen. Ph.D. thesis. TU Bergakademie Freiberg.

Plötze M. and Wolf D. (1996) EPR- und TL-Spektren von Quarz: Bestrahlungsabhängigkeit der $[TiO_4^-/Li^+]^0$-Zentren. *Eur. J. Miner.* **8,** 217.

Poutivcev M., Kempe U., Götze J., Monecke Th., Wolf D. and Kremenetsky A. (2001) Constraints on the genesis of quartz pebbles in Au-U bearing and barren Witwatersrand conglomerates from CL microscopy and trace element analysis (abstract). In *Cathodoluminescence in Geosciences: New Insights from CL in Combination with Other Techniques,* pp. 71–72. Freiberg.

Rakov LT., Milovidova ND., Kuvshinova KA., and Moiseev BM. (1985) EPR investigations of germanium centers in natural polycrystalline quartz (in Russian). *Geokhimiya* **9,** 1339–1344.

Rinneberg H. and Weil J. A. (1972) EPR studies of Ti^{3+}-H^+ centers in X-irradiated alpha-quartz. *J. Chem. Phys.* **56,** 2019–2028.

Roedder E. (1984) *Fluid Inclusions.* Review in Mineralogy 12 646 pp. Mineralogical Society of America.

Rossman G. R., Weis D., and Wasserburg G. J. (1987) Rb, Sr, Nd and Sm concentrations in quartz. *Geochim. Cosmochim. Acta* **51,** 2325–2329.

Schiellerup H., Lambert D. D., Prestvik T., Robins B., McBride J. S., and Larsen B. (2000) Re-Os isotopic evidence for a lower crustal origin of massif-type anorthosites. *Nature* **405,** 781–784.

Schrön W., Baumann L., and Rank K. (1982) Zur Charakterisierung von Quarzgenerationen in den postmagmatogenen Erzformationen des Erzgebirges. *Z. Geol. Wiss.* **10,** 1499–1521.

Schrön W., Schmädicke E., Thomas R., and Schmidt W. (1988a) Geochemische Untersuchungen an Pegmatitquarzen. *Z. Geol. Wiss.* **16,** 229–244.

Schrön W., Oppermann H., Rösler H. J., and Brand P. (1988b) Fest-Gas-Reaktionen als Ursache geo- und kosmochemischer Mobilisierungs- und Anreicherungsprozesse. *Chem. Erde.* **48,** 35–54.

Serebrennikov A. I., Valter A. A., Mashkovtsev R. I., and Shcherbakova M., Ya.. (1982) The investigation of defects in shock-metamorphosed quartz. *Phys. Chem. Miner.* **8,** 153–157.

Smith J. V. (1983) Some chemical properties of feldspars. In *Feldspar Mineralogy. Reviews in Mineralogy 2* (ed. P. H. Ribbe) pp. 281–296. Mineralogical Society of America.

Stavrov O. D., Moiseev B. M., and Rakov L. T. (1978) Investigation of the relation between the concentration of aluminium centers and alkali elements in natural quartz (in Russian). *Geokhimiya* **3,** 333–339.

Stegger P. and Lehmann G. (1989) The structures of three centers of trivalent iron in alpha-quartz. *Phys. Chem. Miner.* **16,** 401–407.

Stockmarr P. (1994) A description of pegmatites at Åvesland and Evje, South Norway (in Danish). M.Sc. thesis. University of Copenhagen, Denmark.

Suščevskaya T. M., Sinjakova S. I., and Markova I. V. (1970) Results of studies about the concentration of ore elements in hydrothermal solutions (in Russian). *Geokhimiya* **6,** 693–700.

Suttner L. and Leininger R. K. (1972) Comparison of the trace element content of plutonic, volcanic and metamorphic quartz from Southwestern Montana. *Geol. Soc. Am. Bull.* **83,** 1855–1862.

Taylor S. R. and McLennan S. M. (1985) *The Continental Crust: Its Composition and Evolution.* Blackwell.

Van den Kerkhof A. M. and Hein U. F. (2001) Fluid inclusion petrography. *Lithos* **55,** 27–47.

Van Moort J. C., Nand A. S., Cohen D. D., Newman S. and Aung P. (1990) The use of electron paramagnetic resonance spectroscopy and trace element content of vein quartz in mineral exploration. In *Exploration Geochemistry 1990* (ed. F. Mrna), pp. 221–228. Proc. 3rd Int. Joint Symp. IAEG and AEG, Geol. Survey, Prague.

Walenczak Z. (1969) Geochemistry of minor elements dispersed in quartz. *Arch. Mineral.* **28,** 189–335.

Watt G. R., Wright P., Galloway S., and McLean C. (1997) Cathodoluminescence and trace element zoning in quartz phenocrysts and xenocrysts. *Geochim. Cosmochim. Acta* **61,** 4337–4348.

Weeks R. A. (1956) Paramagnetic resonance of lattice defects in irradiated quartz. *J. Appl. Phys.* **27,** 1376–1381.

Weil J. A. (1984) A review of electron spin spectroscopy and its application to the study of paramagnetic defects in crystalline quartz. *Phys. Chem. Miner.* **10,** 149–165.

Weil J. A. (1993) A review of the EPR spectroscopy of the point defects in α-quartz: The decade 1982–1992. In *Physics and Chemistry of SiO_2 and the Si-SiO_2 Interface,* Vol. 2 (eds. C. R. Helms and B. E. Deal), pp. 131–144. Plenum Press.

Wright P. M., Weil J. A., Buch T., and Anderson J. H. (1963) Titanium colour centers in rose quartz. *Nature* **197,** 246–248.

Yardley B. W. D., Banks D. A., and Bottrell S. H. (1993) Post-metamorphic good-quartz veins from NW Italy: The composition and origin of ore fluids. *Min. Mag.* **57,** 407–422.